EUROPEAN COMMISSION
5th EURATOM FRAMEWORK PROGRAMME 1998-2002
KEY ACTION : NUCLEAR FISSION

HTR-E

High-Temperature Reactor Components and Systems

CONTRACT N°
FIKI-CT-2001-00177

WP1

Aerodynamic Design – CFD calculations

Deliverable n°9

René Van den Braembussche, Zuheyr Alsalihi, Tom Verstraete
Johan Prinsier, Mickaël Meunier, Grzegorz Kaczmarek, Frits Hannes

von Karman Institute

Belgium

Dissemination level : RE
Document N°: HTR-E 05/08 D-1-2-2
Status : Final
Deliverable n°9

von Karman Institute for Fluid Dynamics INPA
Chaussée de Waterloo, 72
B-1640 RHODE-SAINT-GENESE, BELGIUM.

CONTRACT N°
FIKI-CT-2001-00177

WP1

Helium Turbine Design Study

Deliverable n°9

René Van den Braembussche, Zuheyr Alsalihi, Tom Verstraete
Johan Prinsier, Mickaël Meunier, Grzegorz Kaczmarek, Frits Hannes

von Karman Institute

Belgium

Ref:	VKI CR 2005-45
Date	August 5, 2005
Approved	Rene Van den Braembussche
Visa	

TABLE OF CONTENT

ABSTRACT

-

This report describes the second part of the turbine and compressor design and optimization. It consists of:

1. the further optimization of the compressor and turbine stages described already in ref [1]. This continued optimization has been done in three steps. A first optimization is by reconsidering a combination of loss correlations and stress considerations. It is followed by a manual optimization of the blade shape and blade number by analysing several geometries by means of the 3D Navier Stokes solver in combination with the VKI program for parameterization of the geometry. The third step makes use of the VKI optimization system and is an attempt for further improvements by introducing compound lean.
2. the prediction of the off design performance of the optimized compressor and turbine stage. This calculation is done by analysing the optimized geometry at different mass flows (from 100 kg/sec to 400 kg/sec) in an iterative procedure whereby the distortion of the outlet conditions are superimposed on the inlet conditions to simulate a multistage environment.
3. the calculation of the multistage performance of both the compressor and turbine. This is done by means of a specialized program that first scales the blade height for given inlet conditions and the design mass flow and then calculates the performance in the other operating points. Assumptions are that the pressure ratio and efficiency are function only of the local flow coefficient, and not influenced by the small changes of the (very low) Mach number.

It is shown that the geometry allows achievement of the predicted performance and the overall performance curves of the compressor and turbine are made available for further studies on off design operation and stability of the gas-cooled reactor.

In addition to this, one has also analysed the temperature field on the first turbine stage stator and rotor as well as the heat flux (cooling) required to keep the blade metal temperature at the root section below the critical value of 1173.3 ^{o}K. An estimation of the blade root cooling hole dimensions shows that there is no problem to keep the blade temperature below the critical value.

1. OPTIMIZATION OF THE TURBINE

1.1 The flow analysis codes TRAF3D/TRAFMS

Both turbine and compressor designs and optimizations are based on the results of the 3D Navier Stokes solvers TRAF3D and TRAFMS. These solvers for three-dimensional **TRA**nsonic **F**low in a single **3D** blade row or in a **M**ulti-**S**tage turbine or compressor have been developed in a joint project by the University of Florence and NASA (ICASE and ICOMP) [2].

The TRAF3D predicts the 3D viscous flow in linear and annular cascades with and without tip clearance. The Reynolds-averaged Navier-Stokes equations are solved using a Runge-Kutta scheme in conjunction with accelerating techniques (local time stepping, residual smoothing and **F**ull-**A**pproximation-**S**torage (FAS) multigrid). The equations are discretized using finite volumes and a cell-centered scheme with artificial dissipation. A very low level of artificial viscosity is ensured by eigenvalue scaling, which is a three dimensional extension of the one proposed by Swanson and Turkel [3], and Martinelli and Jameson [4]. The 3D solver can use either C-type or H-type grids. Both grids can handle high stagger or high camber blades by breaking the grid periodicity on the wake to reduce the grid skewness in the throat. The grid generation process is based on an elliptic procedure that solves the discretized Poisson equations using a point relaxation scheme. The three dimensional grid is generated by stacking the two dimensional non-periodic grids.
The two-layer mixing length model of Baldwin and Lomax is used to compute the turbulent quantities. Turbulent flows are assumed on blade and end walls

The multistage program TRAFMS uses circumferential averaging at the interface between stationary and rotating rows. Care has been taken to avoid that this averaging could influence the solution by imposing uniform flow too close to the leading edge. In order to fully account for the impact of the changes in stator geometry the calculations (compressor and turbine) are made with the stator in front of the rotor. Only the H grid is used in the multistage calculations presented here.

1.2 Turbine design considerations

The turbine lay-out proposed in [1] has 12 stages (similar to the GT-MHR) and a load factor Ψ between 2.07 and 2.18 for the central stages. A slightly higher (Ψ =2.19) value is required for the first stage, because of the axial inflow, and a lower value (Ψ = 1.69) at the last stage to obtain axial outlet flow for minimum kinetic energy losses in the ducts.

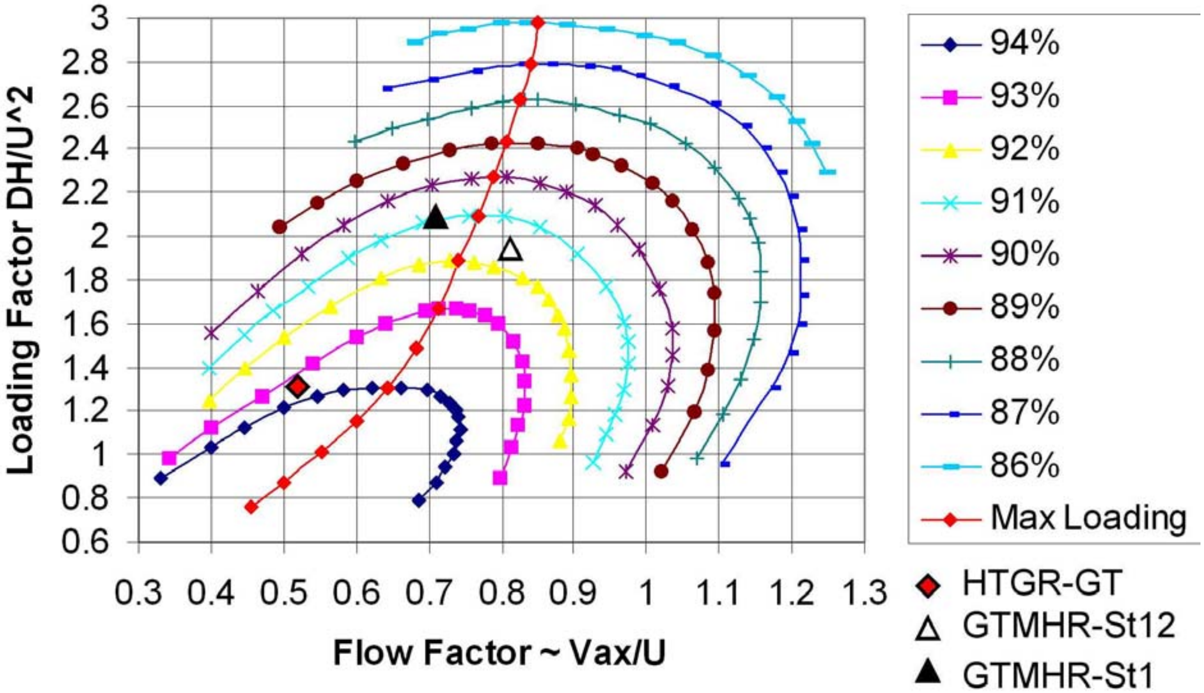

Fig.1. Smith diagram

The Φ value varies between .68 at the inlet to .78 at the outlet. The Smith diagram (Fig 1) shows that under these conditions the maximum efficiency will be around 91% (exclusive tip clearance losses). The reason for this limited efficiency is the high loading resulting from the limited number of stages with a limited peripheral speed. Preliminary performance predictions by means of the Navier Stokes solver TRAF3D indicate rotor-only efficiencies around 93% and confirm that the correlation predicted performance is achievable

The final design is made by analyzing several variants of the turbine geometry by means of the multistage Navier Stokes solver TRAFMS. The hub radius is assumed to be constant and the shroud radius R_S increases to compensate for the decrease of density with the expansion in order to conserve the same Φ and velocity triangles in all stages. This increase of the shroud radius is much smaller for Helium than for air and allows the assumption that all stages will have identical performance (neglecting the effect of the small change in blade height on the secondary flow losses). Hence only one stage has to be optimized.

Stage 2 has been selected for optimization of the turbine. It already has non-uniform inlet conditions and the smallest blade height, hence highest secondary flow losses. The inlet conditions are: listed in table 1.

Table 1. 2nd stage inlet conditions and design target

$P^o{}_{in}$ (Pa)	6553574.5
$T^o{}_{in}$ (°K)	1091.3
α_{in}	35.9
$P^o{}_{out}$ (Pa)	2640000
$T^o{}_{out}$ (°K)	783.2
Pow (MW)	55.5

The inlet total pressure, temperature, non-dimensionalized by there average value, and flow angle variation over the blade height are shown on Fig 2 a and b. They are obtained by superposing the stage outlet flow distortion on the average inlet conditions.

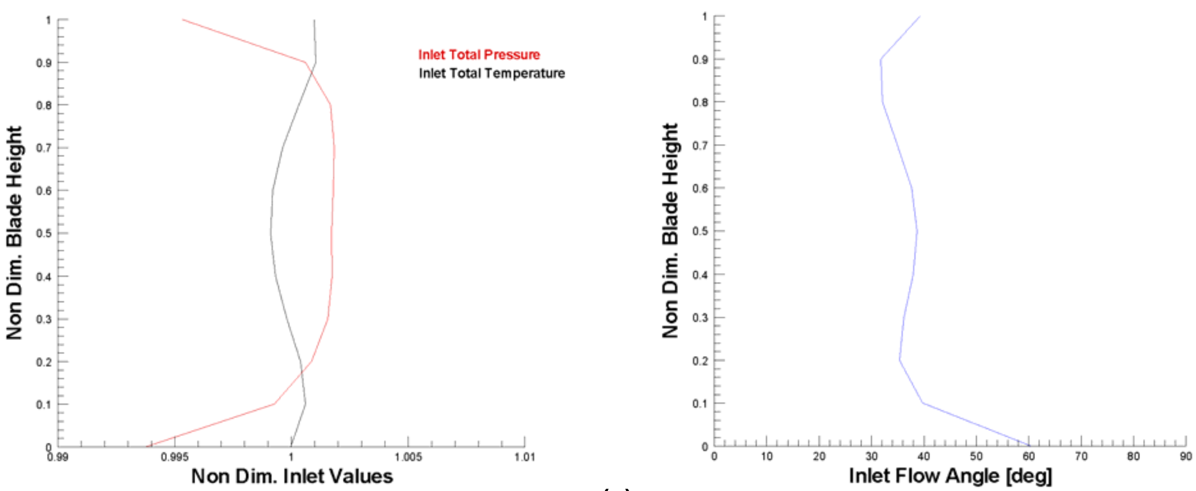

(a) (b)

Fig 2. Non dimensional inlet total pressure and temperature (a) and absolute flow angle

Although the 2D calculations of the stator and rotor blade sections showed very good Mach distributions and low losses, the first 3D calculations indicated efficiencies below the ones predicted by the through flow analysis program. This decrease of performance is attributed to the large secondary losses that are generated in the highly loaded turbine stages ($\Psi > 2.$)

Several modifications of the original blades have been made and verified in an attempt to increase the efficiency.

1.3 Stator blade section redesign

Secondary flows result from the migration of the hub and shroud wall boundary layer from the blade pressure side to the suction side. The consequence is a vortical flow (Fig. 3) and an accumulation of losses in the hub and shroud suction side corner.

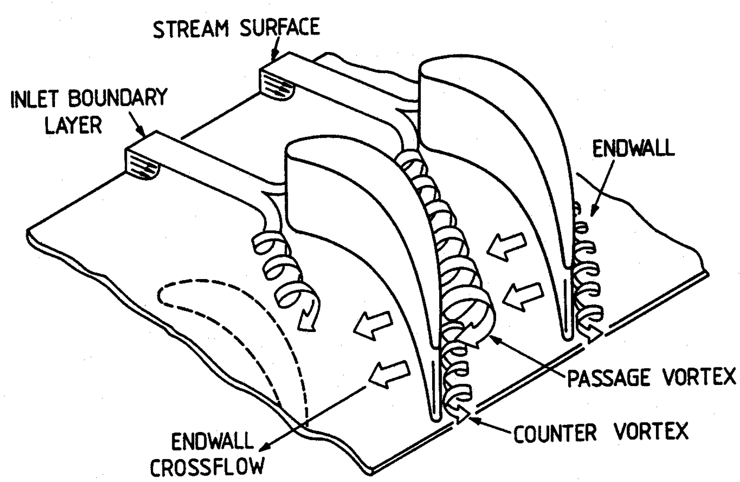

Fig. 3. Secondary flow vorticity

The secondary flows are highest in the stator because of the larger pitch to chord ratio in combination with a high (104. ^{o}) turning. The streamline patterns resulting from these secondary flows are shown on Fig. 4 and 5 respectively for rotor and stator.

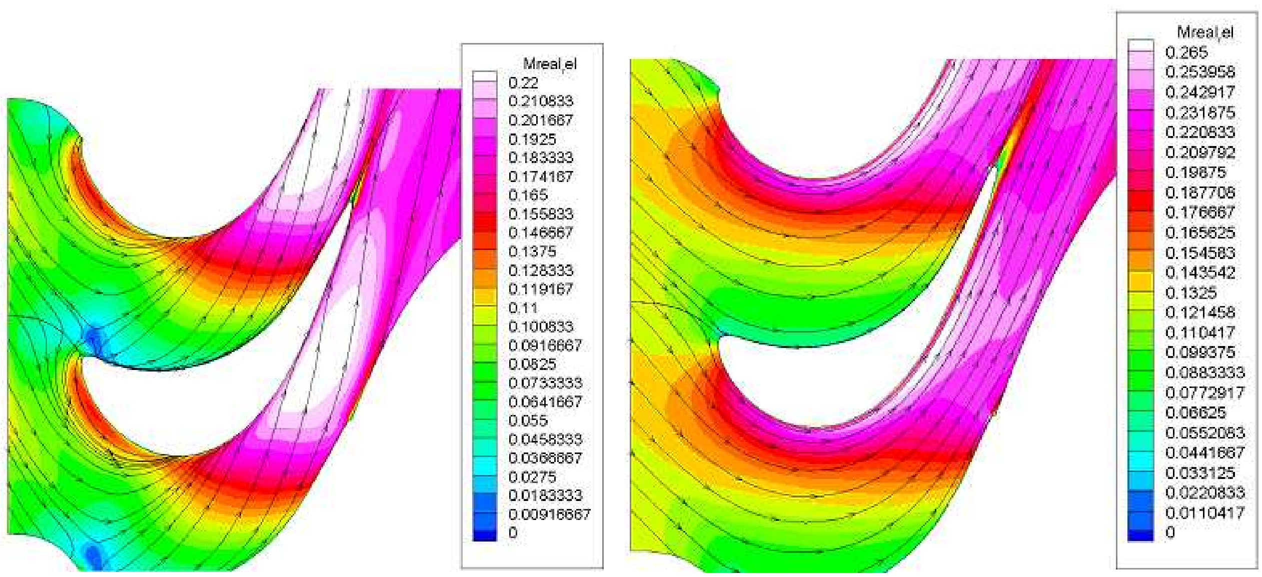

(a) **(b)**

Fig. 4. Streamline pattern in rotor hub (a), and mid section (b)

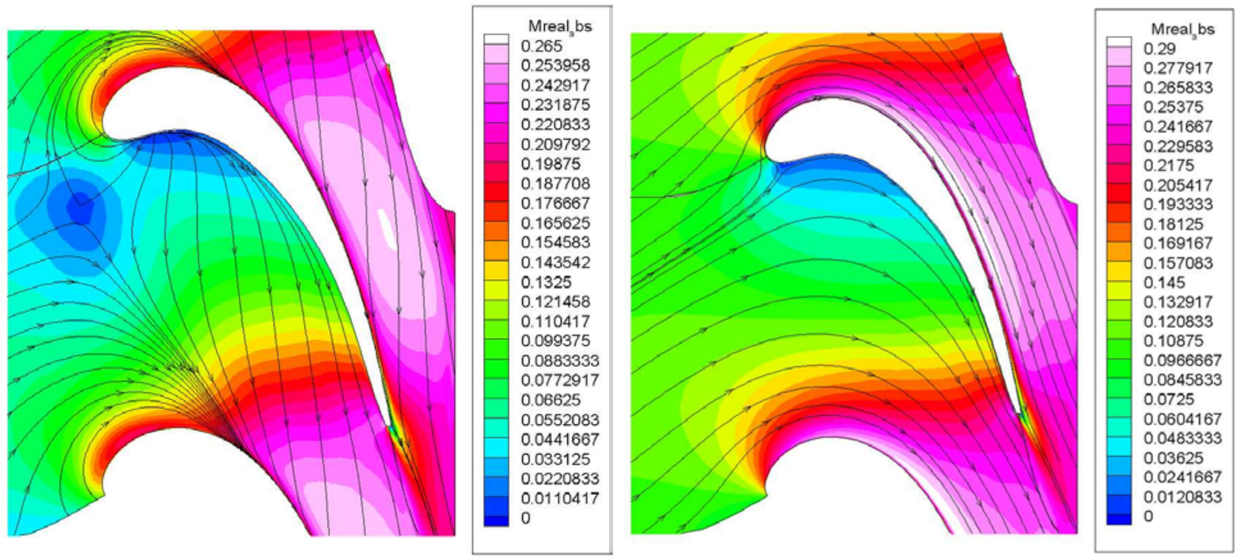

(a) (b)

Fig. 5 Streamline pattern in stator hub (a) and midsection (b).

The streamlines at rotor midsection Fig. 4(b) shows a regular and near optimum pattern. The streamlines near the hub Fig. 4(a) show that the stagnation point has slightly moved to the pressure side and has resulted in some return flows near the leading edge. The situations is much worse in the stator where the return flow near the hub (Fig. 5a) extends over a considerable length of the pressure side. This results in very large secondary flows and hence high losses near the hub. They are the consequence of the increase of the static pressure along the first 20% length of the pressure side (Fig. 6a) resulting in local return flow and a strong horseshoe vortex.

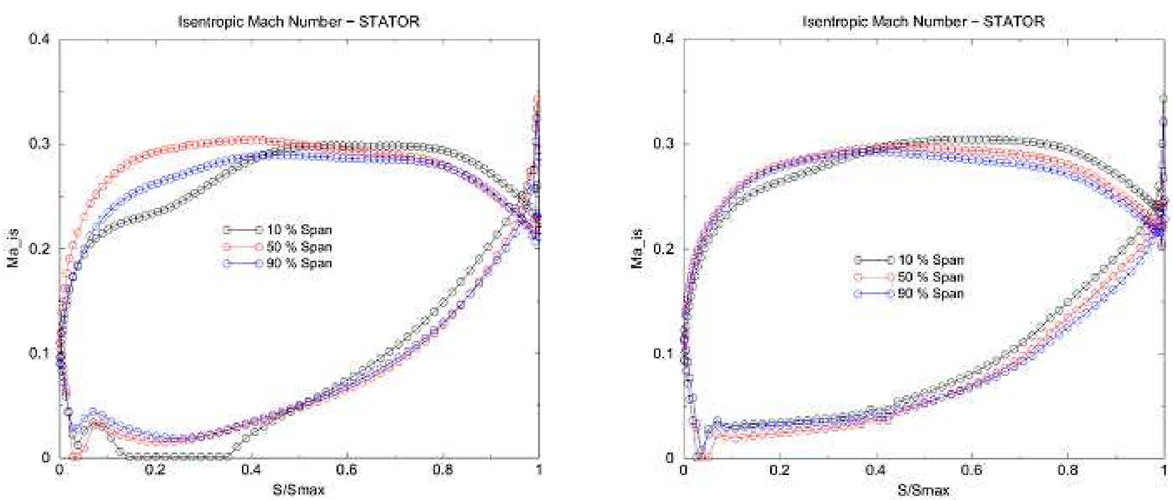

(a) (b)

Fig. 6 Mach number distribution on original (a) and redesigned (b) stator blade for 3D flow in the turbine stage.

Two modifications have been introduced to remediate this problem.

1. a redesign of the blade leading edge to create a decreasing or constant static pressure along the pressure side (Fig. 6b).
2. an increase of the stator blade number from 58 to 77 while keeping the pitch to chord ratio constant. This results in a 25% smaller pitch and chord and a proportional increase of the aspect ratio (blade height over chord).

Both modifications contribute to a reduction of the secondary flow losses.
The old and new blade shape are compared in Fig. 7. One also observes a small reduction of the blade trailing edge thickness. The improvements in Mach number distribution are obvious on Fig. 6b.

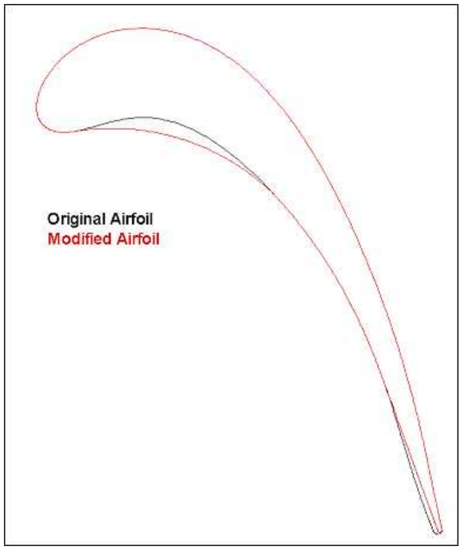

Fig. 7 Original versus new stator blade

The results of the stage analysis with the modified stator blade are compared to those obtained with the original one in table 2. One observes an increase in stage efficiency by 1 % point and an increase in power output by 468.15 kW.

Table 2 : Original versus modified blade main Navier-Stokes results

	Original	Modified
Stage Mean Mass-Flow Rate (kg/s)	300.47	300.57
Stage Power (kW)	43957.01	44425.16
η_{TT} Stage	87.86	88.83
η_{TS} Stator	91.02	91.83
η_{TT} Rotor	93.90	94.39
Stator Turning (deg.)	103.74	103.98
Rotor Turning (deg.)	110.96	111.65
P_{01} (bar) / T_{01} (K)	65.53 / 1091.30	65.53 / 1091.31
P_{02} (bar) / T_{02} (K)	65.23 / 1091.38	65.25 / 1091.33
P_{03} (bar) / T_{03} (K)	60.83 / 1063.16	60.83 / 1062.87

The favorable effect of these modifications becomes clear when comparing the stator, rotor and stage radial distribution of efficiency for the stage with original and redesigned stator (Fig. 8). The shape of the curves is globally the same but the ones with the new stator have shifted to the higher values. For instance, the stator total-to-static efficiency at mid span has increased from an approximate 92.5 % to a little over 95 %, and the stage total-to-total efficiency, at the same radius, has increased from 88 % to 92.5 %. In addition to that one also observes that the low efficiency problems at the stator non-dimensional blade heights of 0.2 and 0.8 have been considerably reduced.

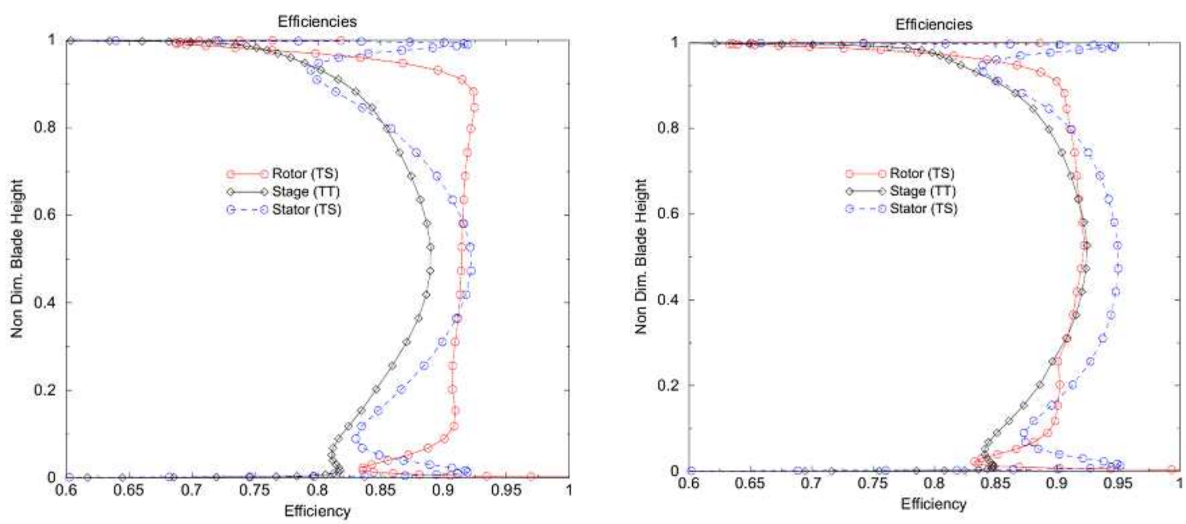

(a) (b)

Fig. 8 Radial variation of efficiencies with original (a) and redesigned stator (b).

The performance of the turbine stage has also been verified by means of other solvers. The NUMECA commercial solver predicts a total to total efficiency of 90.9% whereas the ANSYS commercial solver CFX predicts a 1% point lower efficiency what is in much better agreement with the TRAFMS calculations. Calculations with CFX show a possible increase in efficiency by .7% point when the real gas characteristics of Helium are used.

1.4 3D stator blade optimization

A second way to minimize the secondary flow losses, is by introducing compound lean i.e by bending the blades in the longitudinal direction. The consequence is a variation of the static pressure and a redistribution of the secondary flow losses along the blade span (Fig. 9). This results in an increased blade loading at mid section and a decrease near the end-walls. The problem is to find the optimum bending such that this redistribution of flow and end-wall losses results in a reduction of the overall losses.
Present 3D optimization is limited to the stator only because centrifugal forces could create unacceptable stresses and deformations when leaning the blades of the rotating components.

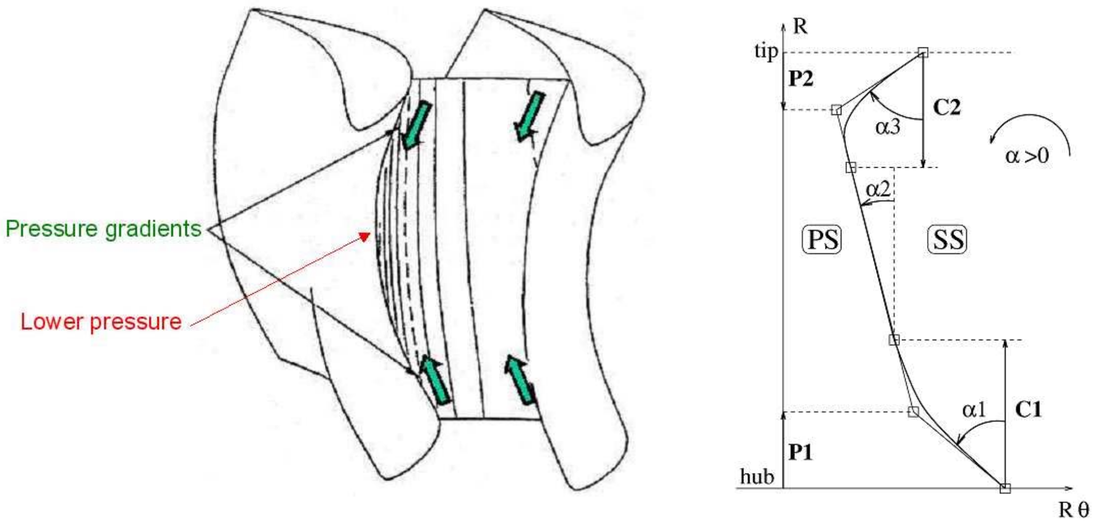

Fig. 9 Compound lean

1.4.1 Optimization method

This redesign is achieved by means of the VKI 3D optimization program [5]

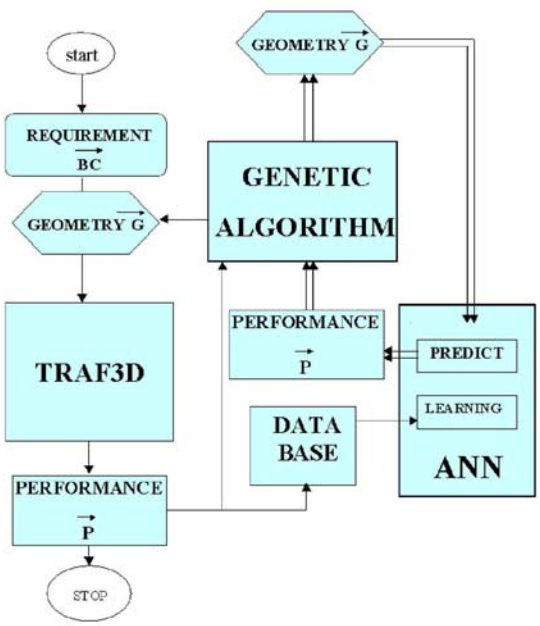

Fig. 10 Flowchart of VKI turbomachinery optimization program

The basic principle of the method is to build an approximate model of the original complicated analysis problem (the two-dimensional Navier-Stokes equations). This approximate model can then be used inside an optimization loop instead of the original model (the two-dimensional Navier-Stokes solver). In this way, the performance evaluations by the approximate model are very fast and the number of evaluations required for the optimization is no longer a critical issue. At the end of this optimization phase, one has recourse to the high-fidelity model to verify the lower-fidelity one. The optimization then continues using again the simplified model after it has been recalibrated by means of the results of the latest Navier Stokes calculation.

The blade design algorithm, of which a flowchart is presented in Fig.10, is composed of 5 processes :

- The design starts with some user-defined inputs : the aerodynamic and mechanical requirements as there are : inlet and outlet flow angles, the outlet static pressure, the Reynolds number, the blade cross-section area and if applicable some mechanical parameters related to the allowable stresses and deformations.
- The second step is the definition of an approximate model of $\vec{P} = N(\vec{BC}, \vec{G})$ relating performance ($\vec{P}$) to the boundary conditions ($\vec{BC}$) and Geometry ($\vec{G}$) by means of an Artificial Neural Networks (ANN). After definition of the unknown parameters of the ANN, called "Learning Process", the neural network is able to generalize, meaning that it can predict the performance of a new blade geometry under given flow-field boundary conditions.
- In the third step, the system uses a Genetic Algorithm (GA) to find the optimum 3D geometry whereby the blade performance is evaluated by an Artificial Neural Network (ANN).
- In the fourth step, the new 3D geometry, provided by the optimizer, is evaluated by the Navier Stokes flow solver. After the flow-field computation, the geometry ($\vec{G}$), boundary conditions ($\vec{BC}$) and performance ($\vec{P}$) of this new sample are added to the DATABASE.
- Finally the performance is checked. If the target performance has not been achieved, a new modification is started and the same process is repeated until convergence to an optimum blade is reached.

As the database grows after each Navier-Stokes computation, improved prediction by the approximate relation $\vec{P} = N(\vec{BC}, \vec{G})$ is expected with time, allowing to locate more precisely the real optimum of the problem.

1.4.2 Parameterized geometry and Database

A critical element in the success of any shape optimization method is its capacity to generate a great variety of different but physically realistic shapes by means of a minimum number of parameters. A parametric definition of the blade geometry is therefore required. The full 3D blade definition makes use of the optimized 2D blade sections and places them along a stacking line defined by 7 parameters (Fig. 9b). The possible design space is restricted by limiting the 7 parameters of the stacking line between the limits defined in table 3.

Table 3 limits of design parameters

	Lower Limit	*Upper Limit*
α_1 (deg)	0	20
α_2 (deg)	-15	15
α_3 (deg)	-20	0
C_1 (percentage of the blade height)	0	0.5
C_2 (percentage of the blade height)	0	0.5
P_1 (percentage of C_1)	0	0.999
P_2 (percentage of C_2)	0	0.999

An optimum spreading of the Database samples over the whole design space is a must to obtain accurate ANN predictions. This is achieved by means of a DOE technique (Design Of Experiment). A full factorial-3 distribution, with a value at 25.% and 75.% of the maximum parameter range, together with a central point (all values in the center of the parameter range) is used for the initial Database.

Some typical geometries are shown on Fig. 11 . One observes a large variety of geometries. The main results of the Navier Stokes calculations on all the Database samples are listed in Table 4. One of the most striking observations in this table is the fact the different geometries give almost the same results as well in terms of efficiency as mass flow as specific power. Variations of efficiency are of the same order as the uncertainty of the Navier Stokes solver.

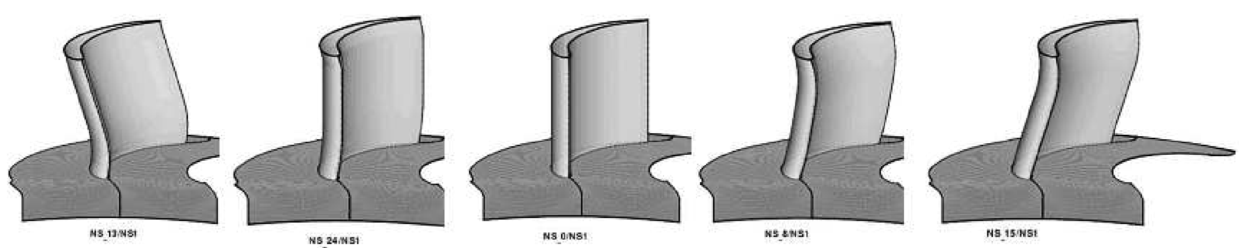

Fig. 11 Typical 3D stator geometries

Table 4: Main Navier-Stokes results of the samples in the Database

CASE	*Mass-flow*	*Stage T-T Efficiency*	*Specific Work*
1	301,20	0,8875	147,38
2	300,94	0,8870	147,41
3	301,31	0,8874	147,47
4	302,17	0,8860	147,02
5	300,87	0,8880	147,61
6	300,97	0,8871	147,41
7	301,63	0,8872	147,40
8	301,98	0,8867	147,17
9	301,46	0,8874	147,37
10	300,87	0,8884	147,78
11	300,77	0,8884	147,81
12	300,82	0,8881	147,74
13	301,30	0,8876	147,51
14	300,89	0,8882	147,75
15	300,77	0,8882	147,79
16	300,92	0,8880	147,63
Central Point	300,80	0,8883	147,79

1.4.4 Results of 3D optimisation

The optimization did not perform as it was expected. Even after 19 optimization cycles it could not find a better geometry than the ones of the Database (Tabel 4). This is even more surprising considering that the same approach resulted in a .3% point improvement in overall efficiency (from 84.16% to 84.48%) when applied to the original non-optimized stator blade.

The only way to find an explanation is by evaluating the effect of the modifications that have been made between these two optimizations. The main reason for not improving the performance may therefore be the larger aspect ratio of the stator blades resulting from an increase of the number of blades from 58 to 77. As a consequence the impact of secondary losses on the overall losses decreases and bending the blades has less influence on it. An other argument is that VKI has often experienced a marginal increase in efficiency when starting 3D optimization from a prismatic blade with well optimized 2D blade shapes. Most spectacular improvements by compound lean in high aspect ratio blades are achieved when starting from blades with low performance, indicating that there was some problem that could be alleviated by bending the blades

As a consequence it turns out that the complication of leaning the improved stator blades does not contribute to a performance improvement and should be abandoned in this design. The maximum achieved performance is the one listed in table 2. Values are in agreement with the Smith correlation (Fig. 1.) taking into account that the correlation does not account for clearance losses.

The coordinates of the optimized turbine stator and rotor are listed in Appendix I. A 3D view on the turbine stage is shown on Fig. 12.

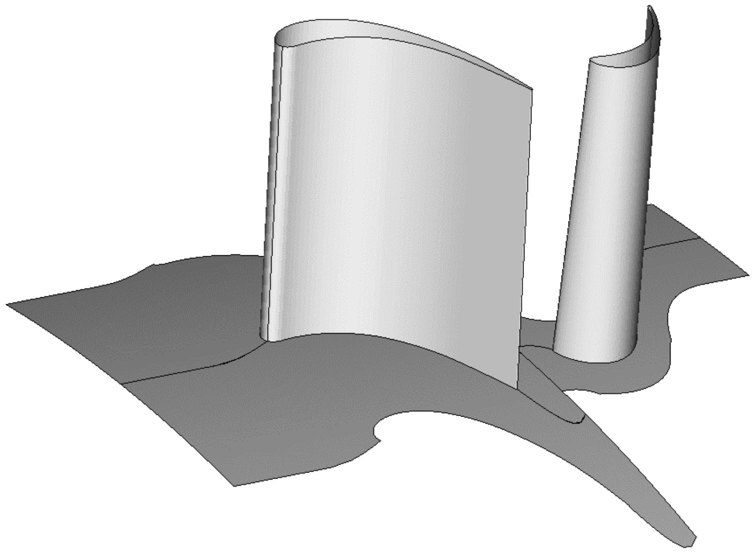

Fig. 12 3D view on optimized turbine stator and rotor.

1.5 Multistage and Off Design performance

The turbine off-design performance is obtained by analysing the optimized turbine stage at different pressure ratio (P^s_{out}/P^o_{in}). This results in a change of mass flow and hence of turbine exit flow conditions. The most important change is in the outlet flow angle. It has to be imposed as inlet conditions for the off-design operation. This is done in an iterative procedure repeating the calculation whereby the inlet conditions are updated until the inlet an outlet flow angles agree.

Table 5 Turbine single stage off design performance

m (kg/s)	P_{01}/P_{03}	α_1 (^{o})	η_{TT} (%)
388.2	1.1431	46.6	81.40
349.8	1.1186	43.2	87.30
338.6	1.1058	41.5	88.00
319.4	1.0952	39.1	88.59
298.8	1.0858	36.0	88.58
282.0	1.0774	32.6	88.45
264.2	1.0697	28.3	88.13
238.0	1.0584	19.6	87.30
191.0	1.0391	-7.	84.30

The off-design performance of stage 2 is listed in table 5. and allows calculation of the multistage performance curve by the following procedure. After selecting a design point mass flow in table 5, one first scales the geometry to locate the design point at the design mass flow (318,6 kg/sec) taking into account that the turbine 2nd stage inlet conditions are different from the turbine design conditions listed in table 2.
The variation of the blade height in the multistage turbine can be defined by imposing that the flow- (Φ), efficiency (η) and load coefficient (Ψ) are the same in every stage from inlet to outlet. The stage pressure ratio and efficiency then allow defining the stage outlet temperature and pressure for given inlet flow conditions. Hence the local density can be calculated and the next stage blade height is obtained by satisfying the continuity in function of the local axial velocity corresponding to the design flow coefficient (Φ). The hub and shroud radius and corresponding blade height of the different stages, defined in this way, are listed in table 6.

Table 6 Multistage turbine geometry (radii and blade height in meter)

R_H	R_S	H
0.78	0.893	0.113
0.78	0.899	0.119
0.78	0.904	0.124
0.78	0.910	0.130
0.78	0.916	0.136
0.78	0.923	0.143
0.78	0.929	0.149
0.78	0.936	0.156
0.78	0.944	0.164
0.78	0.951	0.171
0.78	0.959	0.179
0.78	0.967	0.187
0.78	0.975	0.195

The axial velocity and hence the flow coefficient (Φ) at the off-design operating is calculated from the continuity equation for a prescribed blade height and the off-design mass flow as a function of inlet flow conditions (pressure, temperature and density). Inlet conditions for the second to last stage are again obtained from previous stage outlet conditions. The corresponding flow coefficient (Φ) allows defining the pressure and temperature rise of the next stage by interpolating the single stage performance curve listed in table 5. This procedure is repeated up to the exit of the last stage. The results are listed in table 7 and graphically presented in Fig. 13

Table 7 Multistage performance curve

m (kg/s)	P^o_{out}/P^o_{in}	T^o_{out} (^oK)	η_{TT}	Pow (MW)
106.6	0.851	1065.0	0.805	31.1
203.9	0.631	962.5	0.842	168.2
253.7	0.507	887.7	0.875	307.7
281.6	0.446	844.9	0.892	404.3
300.6	0.409	818.5	0.899	472.8
318.5	0.372	790.8	0.903	546.8
340.5	0.336	763.5	0.902	632.9
360.9	0.299	744.8	0.877	705.9

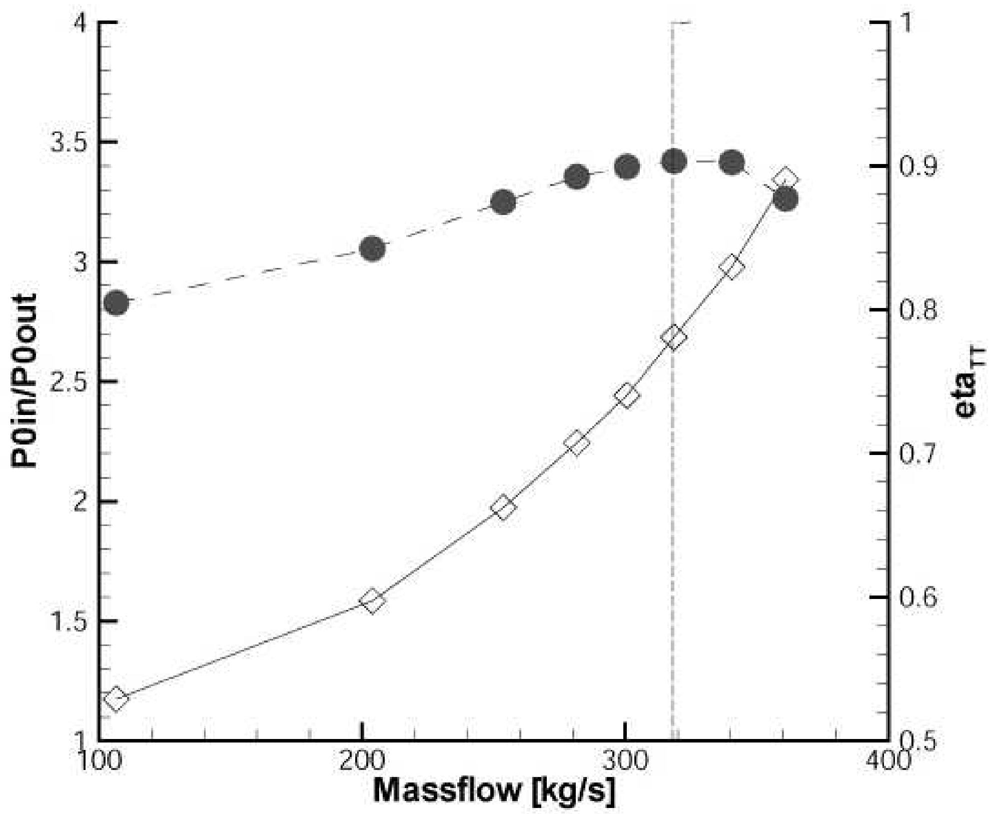

Fig.13 12 stage turbine performance map

The power output at 318.5 kg/s is 546.8 MW and only 8 MW below the target value specified in [1]. This is the consequence of the somewhat lower efficiency (90.3%) of the multistage turbine than the value originally put forward (93.0%) at the start of the layout. This somewhat lower efficiency is mainly the consequence of the very high stage loading and could be remediated by adding one or more stages to lower the loading per stage. However this would make the turbine longer and could cause problems from the rotor-dynamics point of view. Another way to recover the power output, at the predicted efficiency, is by increasing the mass flow by 1.6%.

1.6 Turbine blade cooling

Maximum deformation and creep limits the maximum metal temperature of the turbine to 1023 ^{o}K . Blade root cooling with cold (400. ^{o}K) air from the compressor exit can be used to satisfy this condition. Following iterative procedure has been used to estimate the amount of cooling fluid that is needed for this purpose.

An adiabatic Navier Stokes flow calculation predicts a first estimation of the blade wall temperature. Together with the prescribed maximum temperature at the blade root it provides all the boundary conditions on the blade surface and at the root of the first stage rotor, needed by a finite elements calculation of the heat transfer. The resulting metal temperature on the blade walls is then used as boundary conditions for a non-adiabatic Navier Stokes calculation. The outcome is a more realistic heat flux on the blade walls to be used as boundary condition in the next finite element heat flux calculation inside the blade. This procedure is repeated until convergence i.e. until the wall temperature does not change anymore. The resulting temperature field on the blade wall is shown on Fig 14 for a fluid total inlet temperature of 1091. ^{o}K. The total heat flux is 200. W per blade or a total of 27.5 kW for the first blade row.

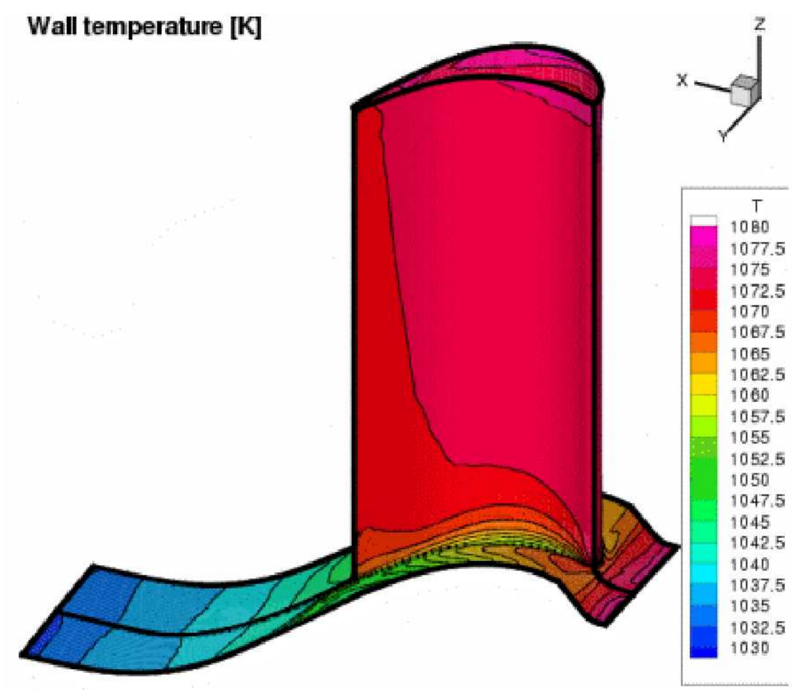

Fig. 14 Stator surface temperature for T^{o}_{in} = 1202 ^{o}K and T_{root} = 1023^{o}K

The total heat transmitted to the blade should be extracted at the blade root. The heat transfer that can be realized in a cooling hole depends on the exchange surface (L*2π*r), the cooling fluid mass flow and temperature.

Two geometries (cooling holes with 5mm and 10mm diameter and 50 mm length) have been analyzed with the cooling gas flow conditions and conductivity k= .187 W/m.K

The heat transfer in a pipe can be approximated by

$$Q(\dot{m}) = h \ \Delta T_{\ln} \frac{\pi D^2 L}{4} \quad (1)$$

where h is the heat transfer coefficient. Its value can be estimated from the Nusselt number, conductivity of the fluid (k) and hydraulic diameter D_H .

$$h = \frac{Nu\ k}{D_H} \quad (2)$$

The Nusselt number for the flow in a pipe can be estimated by the correlation of Dittus-Bölter [6]

$$Nu = .023\ \mathrm{Re}_{D_H}{}^{0.8}\ \mathrm{Pr}^{0.3} \quad (3)$$

for turbulent flows, where

$$\mathrm{Re} = \frac{V\ D_H}{\mu}\rho = f(\dot{m}) \qquad \text{and} \qquad \mathrm{Pr} = 0.7$$

$\Delta T_{\ln}$ is the logarithmic mean temperature difference, function of the fluid inlet (T_{in}=*400.K*) and outlet (T_{out}) temperature and the wall temperature (T_s=*1023.K*).

Assuming a constant wall temperature simplifies the problem and results in the following value of the logarithmic mean temperature difference:

$$\Delta T_{\ln} = \frac{T_{out} - T_{in}}{\ln \dfrac{T_s - T_{out}}{T_s - T_{in}}} \quad (4)$$

Hence the fluid temperature at the outlet of the duct is defined by:

$$T_{out} = T_{wall} - (T_{wall} - T_{in}) e^{\left(\frac{-h \frac{\pi D^2 L}{4}}{\dot{m}\ C_p} \right)} \quad (5)$$

Results of simulations for the two diameters and different values of the cooling flow are summarized in table 8. The heat transfer is per cooling hole and the corresponding mass flow in kg/s is for 137 blades. The pressure drop is based on the assumption that the kinetic energy corresponding to the flow in the hole is completely lost.

Table 8 total heat transfer and mass flow in 77 cooling holes.

diam = 5. mm			diam = 10. mm		
Q (W)	m (kg/s)	ΔP (Pa)	Q (W)	m (kg/s)	ΔP (Pa)
15.7	0.001	0.0	37.8	0.004	0.0
66.2	0.004	1.1	147.8	0.018	1.1
121.7	0.009	4.2	**264.2**	**0.035**	**4.2**
222.5	**0.018**	**16.8**	470.7	0.071	16.8
382.7	0.033	59.2	792.9	0.133	59.2
885.0	0.089	421.1	1781.3	0.354	421.1

Two possible solutions are obvious.

- one hole of 5. mm diameter with a total mass flow of 18. gr/s
- one hole of 10. mm diameter with a total amount of cooling flow of 35 gr./s.

The smaller hole turns out to be more efficient because the higher fluid velocity compensates the smaller cooling surface. The pressure drop is higher but still far below the pressure drop in the first stage (334 Pa). An alternative solution of 2 cooling holes of 5. mm diameter each would require only a 4. Pa pressure drop. However this complication is of no interest because the total amount of cooling fluid is the same and there is more than sufficient pressure difference available. One can conclude from this that the amount of cooling flow is negligible and will not have an impact on the turbine performance.

The main difficulty is the transfer of cooling fluid from the compressor exit stator to the turbine rotor. An incidence free inflow in the rotor requires to accelerate the fluid up to the rotor peripheral speed at the root section. The corresponding kinetic energy is around 250. kPa. The first stator pressure drop is 395. kPa so that the stator outlet static pressure is sufficiently low to create the required cooling flow velocity.

2. OPTIMIZATION OF THE COMPRESSOR

2.1 Compressor design considerations.

The preliminary 1D design and blade definition of the compressor is described in [1]. Proposed is a LP compressor with 15 stages and an HP compressor with 18 stages. The 1D compressor analysis program ACD predicts a total to total efficiency of 88% inclusive the tip clearance losses.
The compressor rotor and stator blades are designed by the VKI inverse design method INVC [7] and analyzed by the 3D Navier Stokes solver TRAF3D. The predicted total to total efficiency is 94.8% and 94.4% respectively for the LP and HP compressor [1]. This is higher than the 1D predictions. These values do not account for clearance losses that are estimated at 1.7% . They also neglect the inlet and outlet duct losses.
In view of these good performances it has not been tried to further improve the 2D blade sections but to improve the overall performance by introducing lean in the stator vanes.

Some preliminary tests have shown that following modifications of the traditional compressor analysis procedure are required to guarantee good predictions.

- a classical compressor analysis starts from a rotor, followed by a stator. It calculates the pressure rise in the stator corresponding to the kinetic energy that is added in the rotor. The main purpose of introducing lean in the stator is a reduction of the secondary flow losses and a more uniform rotor inlet flow. This interaction cannot be evaluated if the rotor is located before the stator because the stator exit conditions do not influence the rotor inlet flow anymore (except by readjusting the rotor inlet conditions in an inaccurate and time consuming iterative way). Following compressor optimizations are therefore done with the stator followed by the rotor.
- the second blade row inlet conditions are defined by circumferentially averaging the first row exit flow angles, total pressure and temperature. However the local static pressure at the interface is influenced by the downstream flow and depends on the circumferential position of the downstream blade row. Hence the downstream stator inlet velocity, function of total and static pressure, depends on the position relative to the downstream blades. Putting the second bladerow sufficiently far downstream should eliminate the influence of the downstream blade on its own inlet conditions. The turbines that have been analyzed in this project (see section 1) have a nearly axial inlet relative velocity and the blade pressure distortion did not extend very far upstream. The real distance between the stator and rotor could be respected in the calculations. The upstream influence of highly staggered compressor blades may be as large as a pitch and a larger distance between the interface and the second row leading edge is required.

All results described in what follows are obtained with the stator upstream of the rotor and with a sufficiently large distance between the blade rows.

2.2 Improved compressor analysis

The compressor has been analyzed with the stator upstream of the rotor and with the distance between the interface and the rotor leading edge increased to 50.% of the rotor chord length. This improved flow analysis confirms that the second stage of the LP compressor reaches a total to total efficiency of 94.% . The HP compressor efficiency will be lower by .2 % point because of the smaller blade height and hence larger secondary flow losses.

The rotor outlet absolute flow distortion is used to define the stator inlet flow conditions for the 3D optimization. They are shown on Fig. 15 a and b. The good agreement between the stator inlet flow- and rotor outlet absolute flow distortion confirms the validity of the multistage calculation procedure that has been used in present study.
A summary of the results is listed in table 10.

Table 10 LP compressor stage performance

	LP compressor
P^o_{in} (Pa)	3 234 711
T^o_{in} (^{o}K)	332.26
α (stator inlet)	55.73
P^o_{out} (Pa)	3 334 888
T^o_{out} (^{o}K)	336.6
m (kg/s)	323.6
η_{TT} (%)	93.97

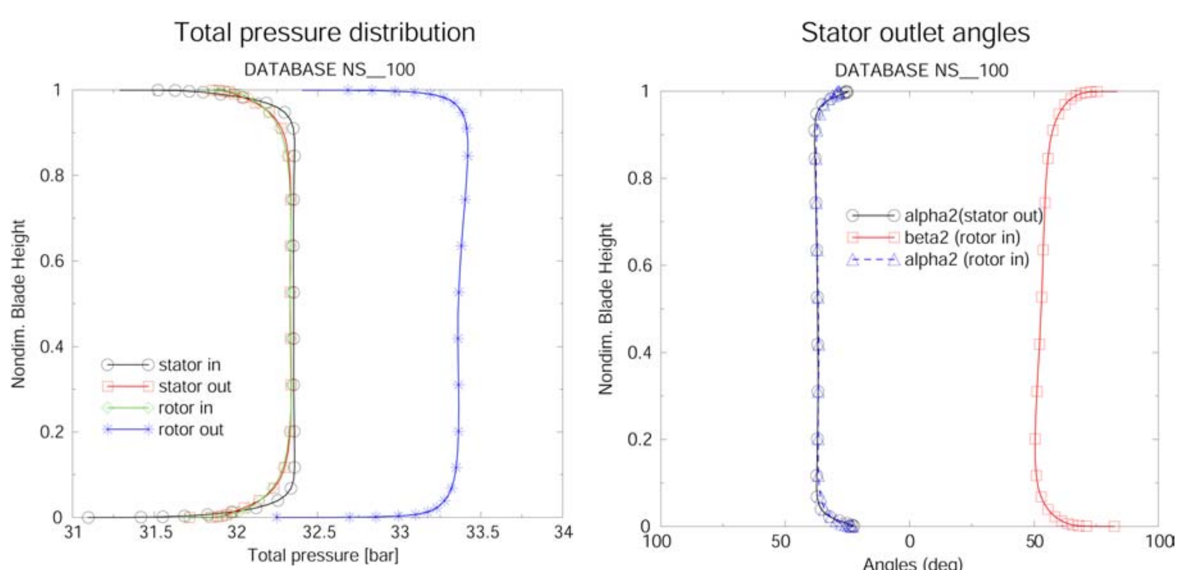

(a) (b)

Fig.15 Stage inlet and outlet total pressure (a) and absolute flow angle (b) distribution

The isentropic Mach number distribution at stator and rotor hub, mean and shroud section are shown on Fig. 16. One observes a very smooth variation of the Mach number at all sections with a limited diffusion along the suction side due to the absence of a high Mach number peak at the leading edge. This together with the low Mach number and large aspect ratio explains the high compressor efficiency. A 3D view on the prismatic stator vane is shown on Fig.17. The rotor vanes are almost identical but mirrored.

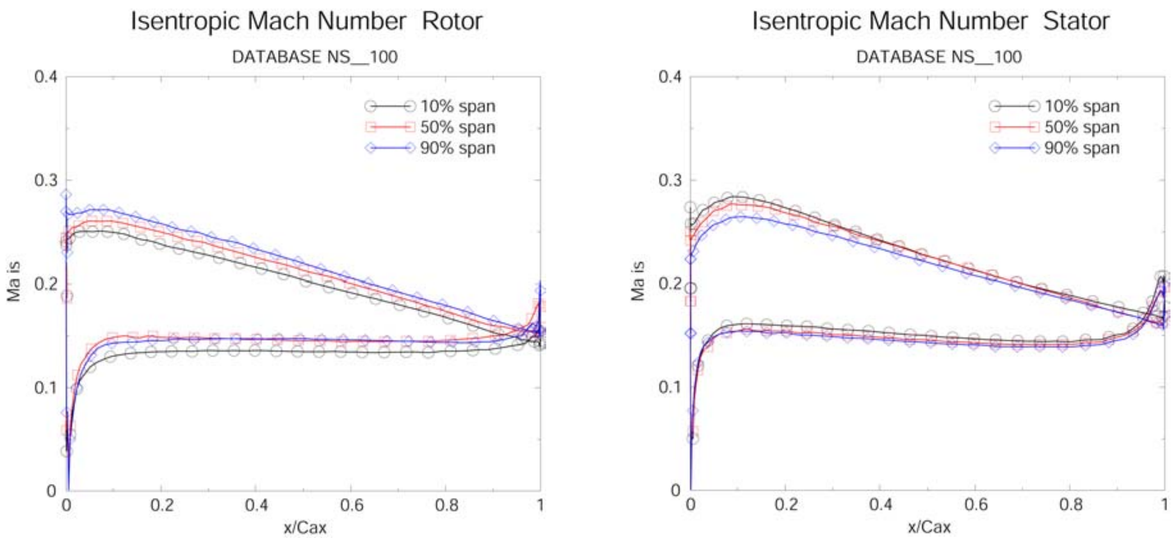

Fig.16 Isentropic Mach number distribution at stator and rotor hub, mean and shroud section.

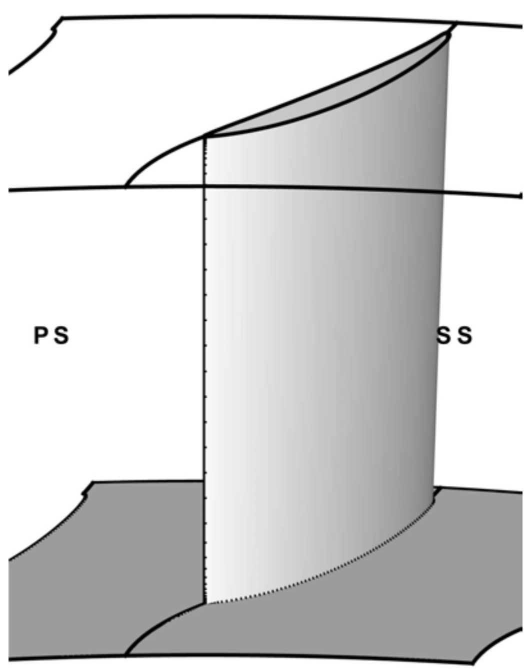

Fig.17 3D view on prismatic stator blade

2.3 3D Compressor blade optimizations

The best prismatic compressor, that has been obtained, is used as starting geometry for the further 3D optimization. This optimization is again made by means of the VKI optimization method used already for the turbine optimization. Assuming that all stages have the same flow, the optimization is limited to Stage 7. The non-uniform inlet conditions of this intermediate stage are again obtained by transposing the outlet distortion of that stage on the average inlet flow conditions. The possible stacking lines are the same as the ones shown on Fig. 9b for the turbine. A DATABASE with 21 samples is created. It is followed by an optimization with 47 iterations (Navier Stokes solutions). The variation of the efficiency is shown on Fig. 18.

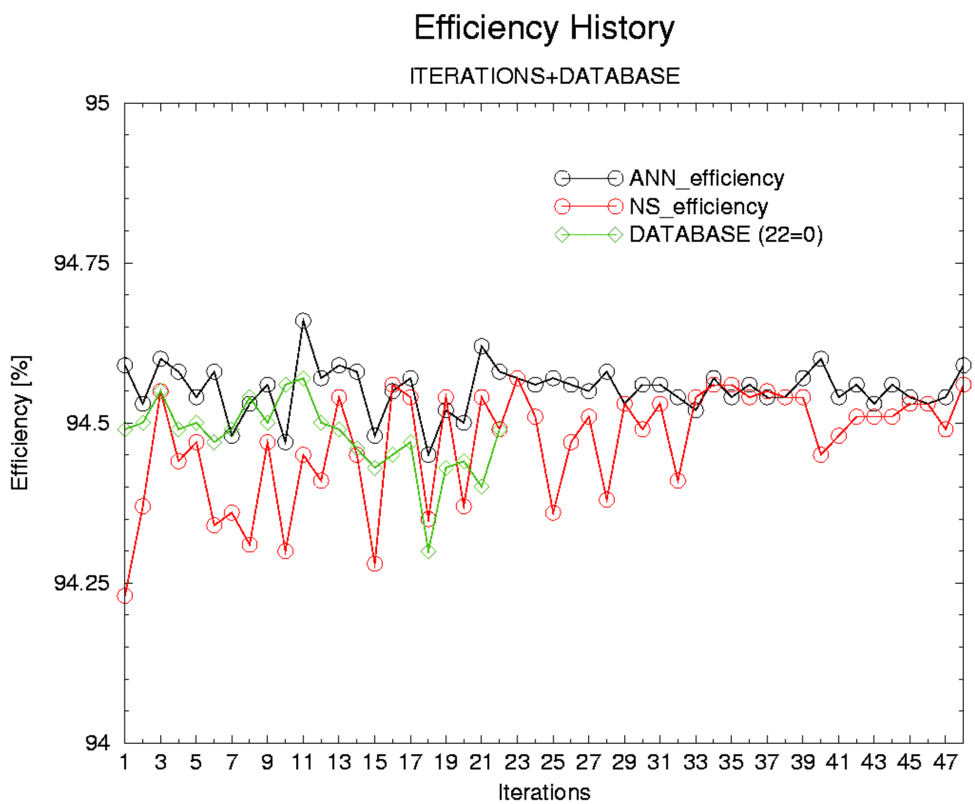

Fig.18 Variation of efficiency during optimization.

The efficiency of the DATABASE samples varies between 94.3 and 94.55. The Navier Stokes predicted efficiency of the best-optimized blade is at iteration 35. The value is 94.55 %. It is only .07% point higher than the initial prismatic blade. The corresponding stator blade geometry is shown on Fig. 19.

A comparison of the streamlines on the suction surface of the prismatic and leaned blade shows the influence of the lean on the secondary flow (Fig. 20). One observes that the streamlines near the shroud and hub wall remain closer to the walls, indicating a weaker secondary flow. However the effect is rather small and so is also the impact on efficiency. It is therefore questionable if the gain with the compound leaned blades is worth the effort of manufacturing much more complex vanes.

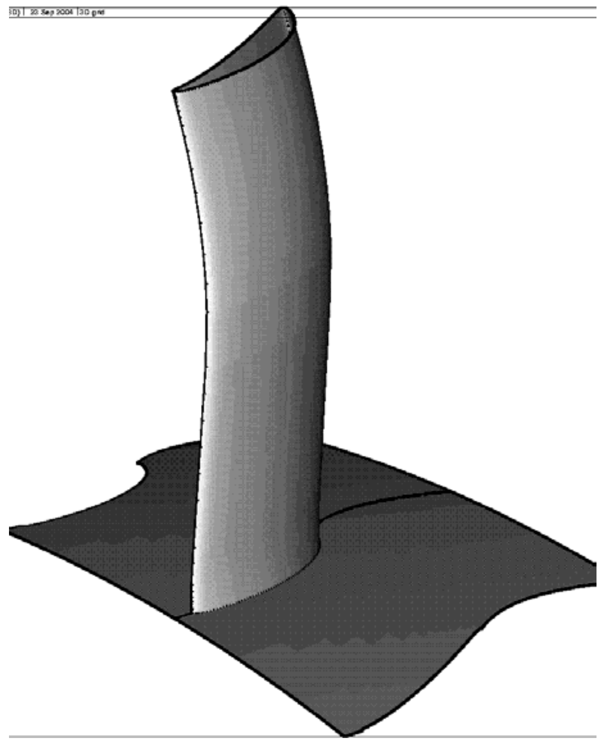

Fig.19 Compound leaned stator blade

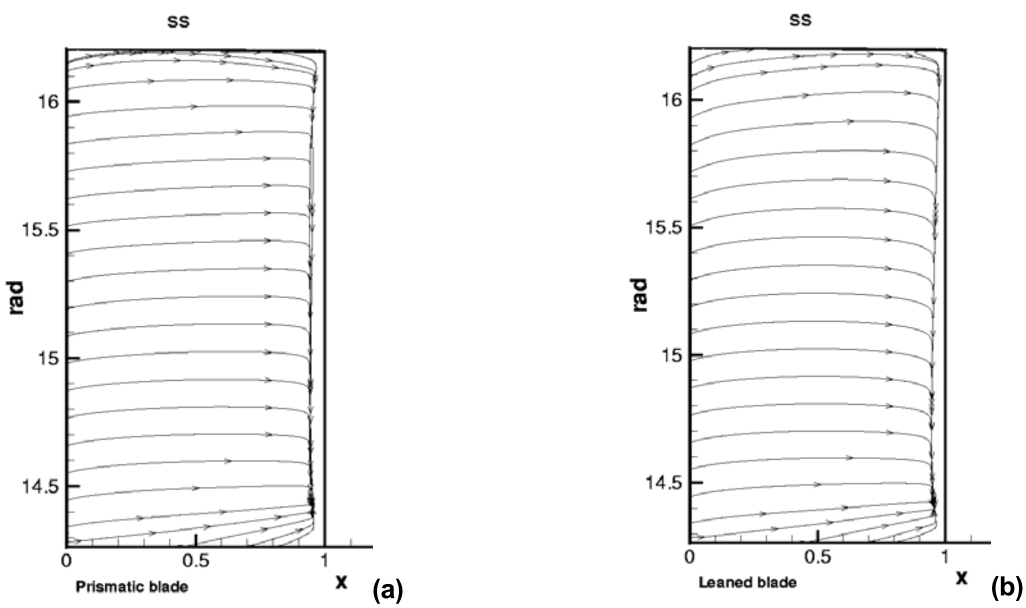

Fig. 20 Suction side streamlines on prismatic (a) and compound leaned (b) stator blade.

Coordinates of the stator and rotor blades are listed in appendix 2.

2.4 Off-design calculations

The compressor off-design performance is obtained by analyzing the optimized compressor stage at different pressure ratios (P^s_{out}/P^o_{in}). This results in a change of mass flow and hence of compressor exit flow conditions. The most important one is the outlet flow angle that has to be imposed as inlet conditions for the off-design operation. This is again done in an iterative procedure until the value of the inlet and outlet flow angle agree.
All calculations are made with .25 mm rotor tip clearance and zero stator clearance, assuming a shrouded stator. The rotor clearance is very small and unlikely to be achievable. A more realistic rotor clearance and the leakage flow in the stator shroud seal will result in a reduction of the efficiency by 1.5% for the LP and HP compressor (assuming 1. mm clearance).
The efficiencies, calculated at all operating points, are reduced for tip clearance losses and the pressure ratio is adjusted assuming that the work input remains unchanged when increasing the clearance. The corrected performance of the 7th stage of the LP compressor is listed in table 9.

Table 9 Compressor stage off-design performance

mass fl. (kg/s)	η_{TT}	P_{02}/P_{01}
409.34	0.863	1.018
382.94	0.898	1.022
354.38	0.916	1.026
323.55	0.925	1.031
289.75	0.922	1.035
252.53	0.898	1.037
153.91	0.800	1.036

2.5 Multistage performance

The multistage performance is calculated in the same way as explained for the turbine. The performance calculated at the seventh stage inlet conditions is first scaled to the compressor inlet conditions. The overall results of the multistage compressors are listed in table 10. The LP inlet conditions are the ones given by the design specifications. The HP compressor inlet total pressure is calculated as a function of the LP outlet conditions assuming a 60 000 Pa total pressure drop in the intercooler. The HP compressor inlet temperature is defined by the intercooler outlet temperature at 301 ^oK.
The predicted total power needed to drive the compressors at design mass flow is 274.5 MW . This is 22.3 MW less than estimated in [1]. This is a consequence of the higher efficiency per stage resulting from a limited loading per stage. This lower load per stage has also resulted in the need to increase the number of HP stages from 18 to 21 to reach the required overall pressure ratio.

Table 10 Overall performance of the LP and HP compressor

	LP (15 stages)	HP (21 stages)
P_{0in} (Pa)	2 550 000.	4 340 000.
T_{0in} (^oK)	299.0	301.0
P_{0out} (Pa)	4 409 066	7 960 272
T_{0out} (^oK)	376.8	389.0
m (kg/s)	318.5	318.5
Power (MW)	129.10	145.89

The calculated values of the 15 stage LP compressor off design performance are listed in Table 11 and plotted on Fig. 21

Table 11 LP compressor off-design performance summary

m (kg/s)	P_{0out}/P_{0in}	T_{0out}	η_{TT}	Power (MW)
118.26	1.7100	395.08	0.744	59.041
212.45	1.7858	392.21	0.837	102.898
281.79	1.7741	382.54	0.922	122.315
318.50	**1.7312**	**377.01**	**0.940**	**129.100**
351.32	1.6119	366.08	0.937	122.446
381.90	1.5106	357.14	0.922	115.368
410.96	1.3874	348.37	0.847	105.424
438.69	1.1914	339.87	0.531	93.164
118.26	1.7100	395.08	0.744	59.041

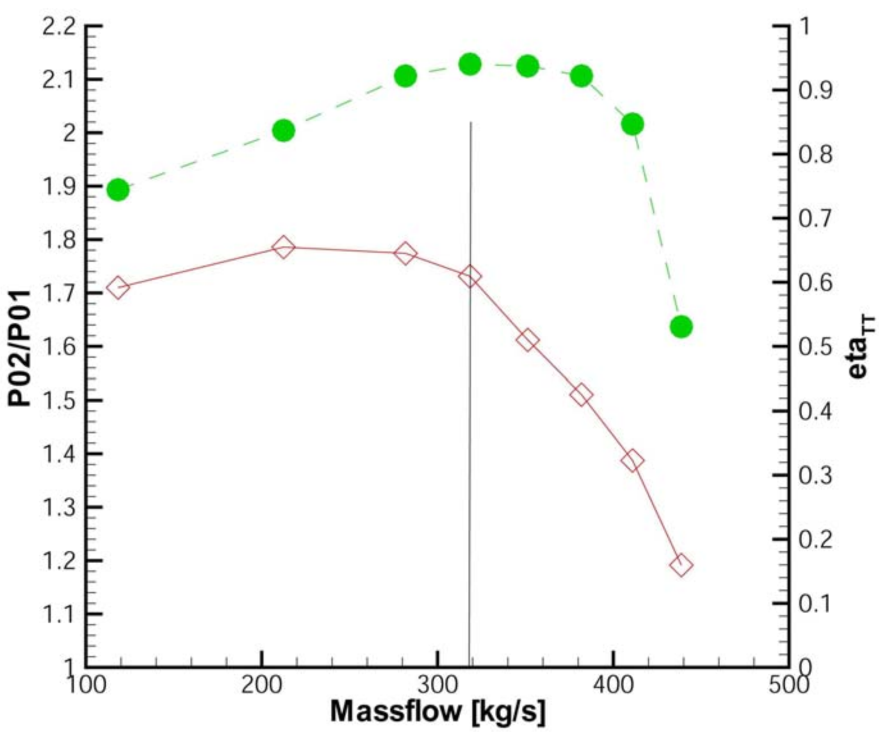

Fig. 21 LP compressor performance map

Fig. 21 shows a rather flat pressure rise curve with a large operating range. The maximum mass flow is around 450 kg./sec. The surge point can be estimated at 200 kg/sec where maximum pressure ratio is observed. This large range is a consequence of the limited stage loading and the low Mach numbers that occur in Helium compressors.

The variation of the LP compressor shroud radius and blade height is listed in table 12. Section 1 is the inlet section "exit" is the outlet section of stage 15.

Table 12 Multistage LP compressor geometry (radii and blade height in meter)

stage Nr.	R_H (m)	R_S (m)	Heigth (m)
1 = inlet	0.7863	0.9228	0.1365
2	0.7863	0.9200	0.1337
3	0.7863	0.9173	0.1310
4	0.7863	0.9147	0.1284
5	0.7863	0.9122	0.1259
6	0.7863	0.9098	0.1235
7	0.7863	0.9075	0.1212
8	0.7863	0.9052	0.1189
9	0.7863	0.9031	0.1168
10	0.7863	0.9010	0.1147
11	0.7863	0.8989	0.1126
12	0.7863	0.8970	0.1107
13	0.7863	0.8951	0.1088
14	0.7863	0.8932	0.1069
15	0.7863	0.8914	0.1051
exit	0.7863	0.8897	0.1034

The 21 stages HP compressor off design performance is listed on Table 13 and plotted on Fig. 22. The surge and choking limits agree well with the LP compressor value. The best efficiency is again at the design point mass flow. The steeper slope of the pressure rise curve is the consequence of the larger number of stages than in the LP compressor.

Table 13 HP compressor performance

m (kg/s)	P_{0out}/P_{0in}	T_{0out}	η_{TT}	Power (MW)
107.22	1.9597	427.28	0.736	70.349
192.61	2.0664	423.51	0.827	122.606
255.47	2.0497	410.80	0.911	145.743
288.75	1.9971	403.53	0.935	153.826
318.50	**1.8354**	**389.16**	**0.938**	**145.899**
346.22	1.6938	377.41	0.924	137.464
372.57	1.5373	365.89	0.870	125.616
397.71	1.2428	354.72	0.509	111.008
107.22	1.9597	427.28	0.736	70.349

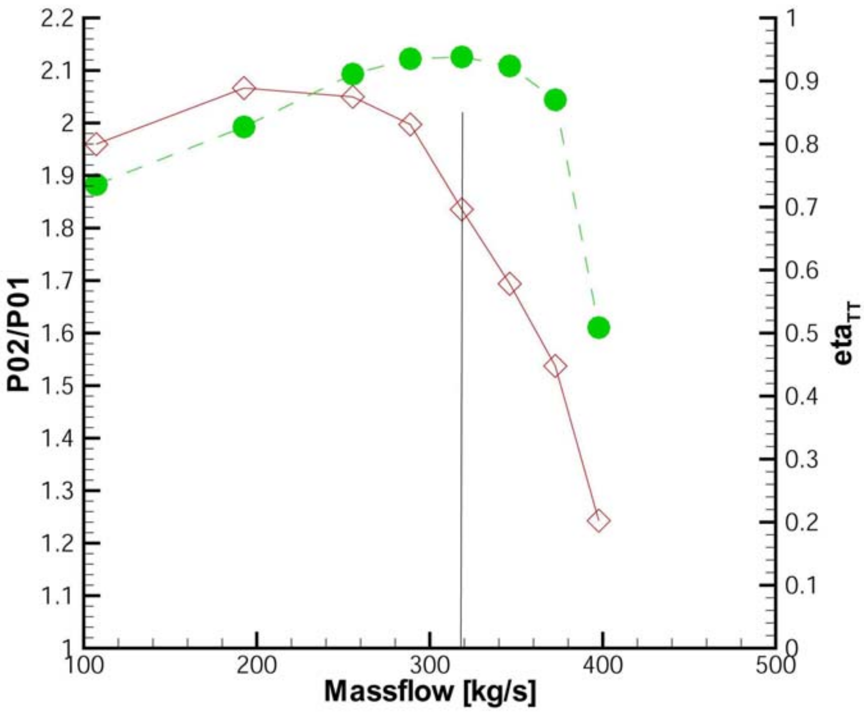

Fig. 22 HP compressor performance map

Table 14 Multistage HP compressor geometry (radii and blade height in meter)

stage Nr.	R_H (m)	R_S (m)	Heigth (m)
1 = inlet	0.786	0.865	0.0784
2	0.786	0.863	0.0771
3	0.786	0.862	0.0758
4	0.786	0.861	0.0745
5	0.786	0.860	0.0733
6	0.786	0.858	0.0720
7	0.786	0.857	0.0709
8	0.786	0.856	0.0697
9	0.786	0.855	0.0686
10	0.786	0.854	0.0676
11	0.786	0.853	0.0665
12	0.786	0.852	0.0655
13	0.786	0.851	0.0645
14	0.786	0.850	0.0636
15	0.786	0.849	0.0626
16	0.786	0.848	0.0617
17	0.786	0.847	0.0609
18	0.786	0.846	0.0600
19	0.786	0.845	0.0591
21	0.786	0.845	0.0583
exit	0.786	0.844	0.0575

The variation of the HP compressor shroud radius and blade height is listed in table 12. Section 1 is the inlet section exit is the outlet section of stage 21.

3. CONCLUSIONS

The previous calculations have shown that leaning the compressor or turbine blades (full 3D design) does not substantially contribute to more power input or higher efficiency of the gas turbine. It is probably not worth the complication. The main reason is the high performance of the optimized 2D blade sections and the correct stacking of them.

The compressor performance exceeds the requirements and initial predictions. The main reason is the careful blade design with rather low loading. This low loading results in a larger number of stages (21 instead of 18 for the HP compressor). This increases the shaft length and could eventually lead to rotor-dynamic problems.

The turbine efficiency is lower than the initial target value. This is a direct consequence of the small number of stages at 3000 RPM. Increasing the number of stages or increasing the rotational speed to 3600 RPM would allow lower loading per stage, hence higher efficiency as clearly shown by the Smith correlation. Here again, more stages would increase the shaft length and could eventually lead to rotor-dynamic problems.

The amount of cooling flow needed to keep the first turbine rotor root below a given maximum temperature is very small and without measurable impact on the gasturbine efficiency. One single hole in the blade root of 5 to 10 mm diameter is sufficient.

The global power output of the gasturbine (turbine –compressor) at nominal mass flow is:

$$546.8-129.1-145.9 = 271.8 \text{ MW}$$

This is a 9.3 MW above the predictions in [1]. The lower turbine output has been more than compensated by a smaller compressor power.

Bibliography.

[1] Brouckaert J.F., Van den Braembussche R.A., Helium Turbine Design Study, FIKI-CT-2001-100177, *Document No: HTR-E 03/12 D-1-1-5-1*

[2] Arnone A., Liu M-S. & Povinelli L.A., 1992: "Navier-Stokes Solution of Transonic Cascade Flows using Non-periodic C-Type Grids". *Journal of Propulsion and Power*. Vol. 8, No. 2.

[3] Swanson R.C.& Turkel E.; Artificial Dissipation and Central Difference Schemes for the Euler and Navier Stokes Equations, *AIAA Paper 87-1107*, June, 1987,

[4] Martinelli L. & Jameson A.; Validation of a Multi-grid Method for the Reynolds Averaged Equations, *AIAA Paper 88-0414*, 1988

[5] Pierret S.; Designing Turbomachinery Blades by means of the Function Approximation Concept Based on Artificial Neural Network, Genetic Algorithm and the Navier Stokes Equation, *PhD. thesis*, VKI 1999.

[6] Dittus F.W. & Bölter,: University of California Publications on Engineering 2 (1930), p. 433.

[7] R.A. Van den Braembussche, An Inverse Design Method for Cascade Blades with Prescribed Velocity Distribution, *VKI CR. 1988-20, Theory and manual*, Reprint 1989,

Appendix I Coordinates of the optimized turbine stator and rotor

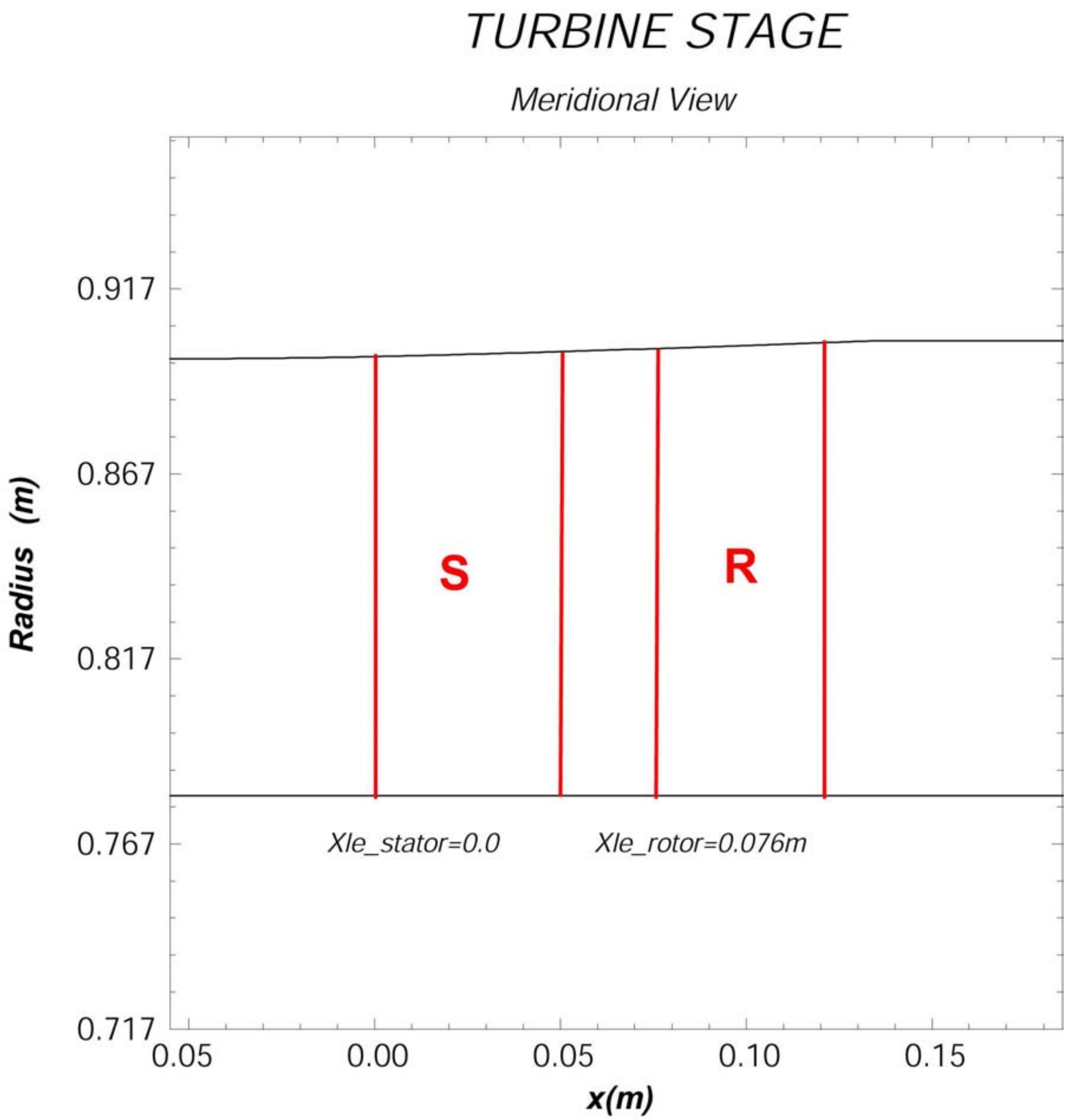

The turbine hub and shroud coordinates x and R (m) are listed in following table. Xle_stator and Xle_rotor are the position of the stator and rotor leading at the hub

x(hub)	R(hub)
-0.084468	0.78
-0.079836	0.78
-0.075464	0.78
-0.071328	0.78
-0.067410	0.78
-0.06369	0.78
-0.060150	0.78
-0.056776	0.78
-0.053551	0.78
-0.050463	0.78
-0.047498	0.78
-0.044645	0.78
-0.041893	0.78
-0.039232	0.78
-0.036652	0.78
-0.034145	0.78
-0.031704	0.78
-0.029322	0.78
-0.026991	0.78
-0.024706	0.78
-0.022462	0.78
-0.020253	0.78
-0.018075	0.78
-0.015923	0.78
-0.013795	0.78
-0.011686	0.78
-0.009593	0.78
-0.007515	0.78
-0.005447	0.78
-0.003388	0.78
-0.001336	0.78
0.0007102	0.78
0.0027541	0.78
0.0047962	0.78
0.0068377	0.78
0.0088800	0.78
0.0109241	0.78
0.0129707	0.78
0.0150207	0.78
0.0170747	0.78
0.0191334	0.78
0.021197	0.78
0.0232661	0.78
0.0253408	0.78
0.0274214	0.78
0.029508	0.78
0.0316006	0.78
0.0336992	0.78
0.0358038	0.78
0.0379141	0.78
0.0400299	0.78
0.042151	0.78
0.044277	0.78
0.0464076	0.78
0.0485423	0.78
0.0506806	0.78
0.052822	0.78
0.0549659	0.78
0.0571116	0.78
0.0592585	0.78
0.0614059	0.78
0.0635531	0.78
0.0656992	0.78
0.0678434	0.78
0.0699848	0.78
0.0721227	0.78
0.074256	0.78
0.0763838	0.78
0.0785052	0.78
0.0806191	0.78
0.0827246	0.78
0.0848207	0.78
0.0869062	0.78
0.0889802	0.78
0.0910416	0.78
0.0930893	0.78
0.0951222	0.78
0.0971393	0.78
0.0991393	0.78
0.101121	0.78
0.103084	0.78
0.105026	0.78
0.106947	0.78
0.108845	0.78
0.110718	0.78
0.112567	0.78
0.114389	0.78
0.116183	0.78
0.117947	0.78
0.119681	0.78
0.121381	0.78
0.123048	0.78
0.124678	0.78
0.126271	0.78
0.127822	0.78
0.129331	0.78
0.130795	0.78
0.13221	0.78
0.133574	0.78
0.134882	0.78
0.29976	0.78

X(shroud)	R(shroud)
-0.084468	0.8981
-0.0798367	0.8981
-0.0754641	0.8981
-0.0713286	0.898101
-0.0674102	0.898102
-0.06369	0.898105
-0.0601508	0.898109
-0.0567763	0.898114
-0.0535519	0.898121
-0.0504636	0.898129
-0.0474988	0.898138
-0.0446457	0.89815
-0.0418934	0.898163
-0.0392321	0.898177
-0.0366524	0.898194
-0.0341459	0.898212
-0.0317049	0.898232
-0.0293223	0.898254
-0.0269916	0.898278
-0.0247066	0.898304
-0.0224622	0.89833
-0.0202531	0.89836
-0.018075	0.89839
-0.0159236	0.898422
-0.0137952	0.898456
-0.0116863	0.898491
-0.0095939	0.898527
-0.0075152	0.898565
-0.0054476	0.898605
-0.0033888	0.898646
-0.0013368	0.898688
0.00071027	0.898732
0.00275414	0.898776
0.0047962	0.898822
0.00683778	0.89887
0.00888007	0.898918
0.0109241	0.898967
0.0129707	0.899017
0.0150207	0.899069
0.0170747	0.899121
0.0191334	0.899175
0.021197	0.899229
0.0232661	0.899284
0.0253408	0.899341
0.0274214	0.899397
0.029508	0.899456
0.0316006	0.899515
0.0336992	0.899574
0.0358038	0.899635
0.0379141	0.899695
0.0400299	0.899758
0.042151	0.89982
0.044277	0.899883
0.0464076	0.899947
0.0485423	0.900012
0.0506806	0.900078
0.052822	0.900143
0.0549659	0.90021
0.0571116	0.900277
0.0592585	0.900345
0.0614059	0.900413
0.0635531	0.900482
0.0656992	0.90055
0.0678434	0.90062
0.0699848	0.90069
0.0721227	0.90076
0.074256	0.900831
0.0763838	0.900902
0.0785052	0.900973
0.0806191	0.901044
0.0827246	0.901115
0.0848207	0.901188
0.0869062	0.901259
0.0889802	0.901331
0.0910416	0.901402
0.0930893	0.901474
0.0951222	0.901545
0.0971393	0.901617
0.0991393	0.901688
0.101121	0.901758
0.103084	0.901829
0.105026	0.901898
0.106947	0.901968
0.108845	0.902037
0.110718	0.902105
0.112567	0.902173
0.114389	0.902239
0.116183	0.902305
0.117947	0.90237
0.119681	0.902434
0.121381	0.902498
0.123048	0.902559
0.124678	0.90262
0.126271	0.90268
0.127822	0.902737
0.129331	0.902794
0.130795	0.902848
0.13221	0.902902
0.133574	0.902953
0.134882	0.903002
0.29976	0.903002

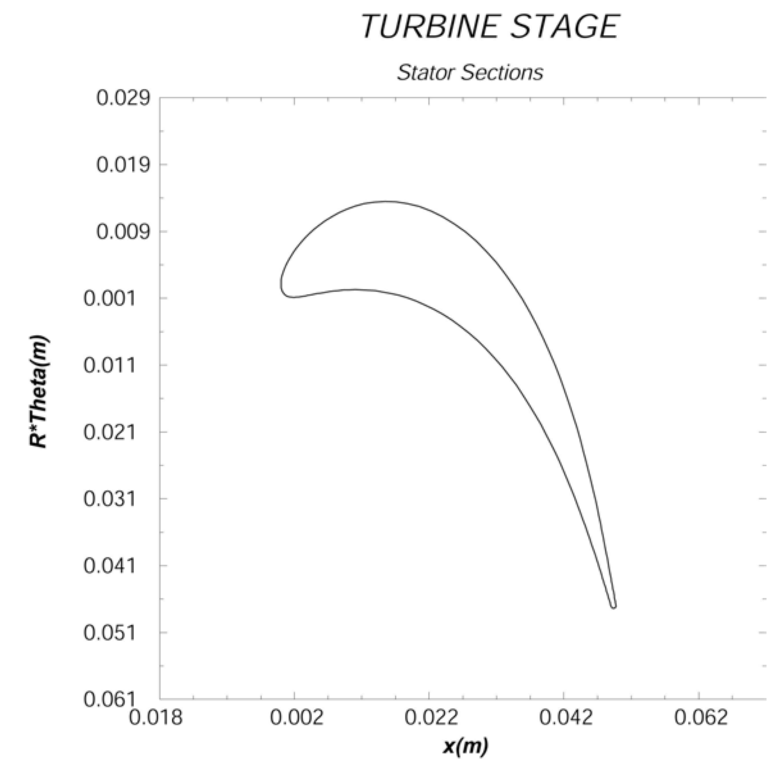

Turbine stator blade

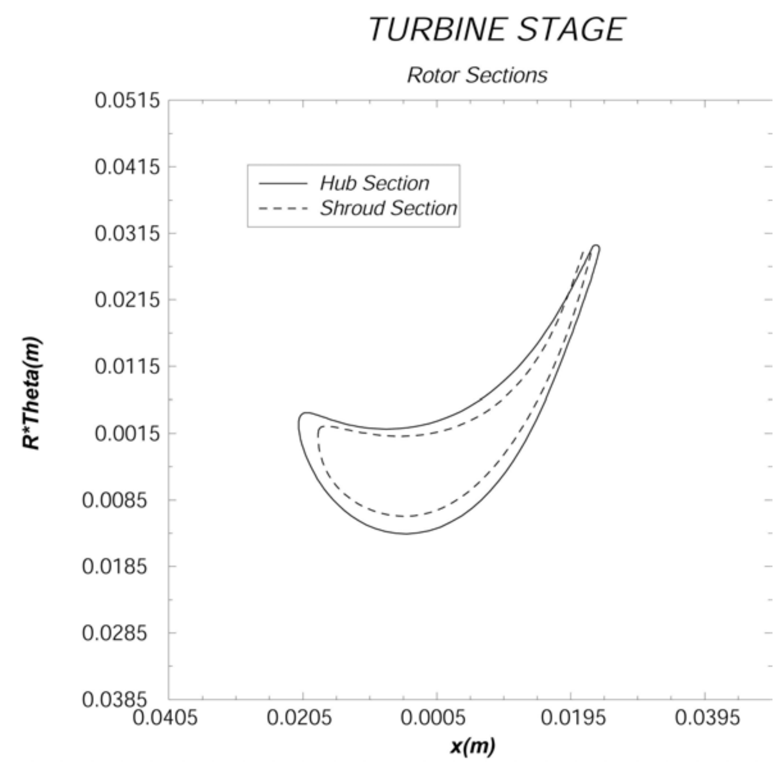

Turbine rotor blade

The turbine stator blade coordinates are listed in following table
(x and R*theta in m) located at Hub (R=0.779)

101 nr of points on suction side

0.000247	0.000000	0.010991	0.012790	0.046933	-0.032388
0.000203	0.000091	0.012369	0.013160	0.047182	-0.033562
0.000160	0.000194	0.013852	0.013410	0.047411	-0.034665
0.000120	0.000309	0.015431	0.013513	0.047621	-0.035701
0.000084	0.000436	0.017088	0.013445	0.047815	-0.036672
0.000052	0.000577	0.018802	0.013186	0.047993	-0.037578
0.000026	0.000733	0.020550	0.012726	0.048156	-0.038424
0.000009	0.000903	0.022303	0.012062	0.048307	-0.039212
0.000000	0.001092	0.024043	0.011196	0.048445	-0.039945
0.000003	0.001294	0.025747	0.010141	0.048572	-0.040626
0.000018	0.001516	0.027400	0.008912	0.048689	-0.041257
0.000047	0.001759	0.028991	0.007526	0.048797	-0.041842
0.000091	0.002017	0.030509	0.006003	0.048896	-0.042383
0.000153	0.002297	0.031953	0.004360	0.048987	-0.042885
0.000234	0.002599	0.033317	0.002617	0.049071	-0.043347
0.000336	0.002923	0.034601	0.000791	0.049148	-0.043773
0.000462	0.003270	0.035804	-0.001098	0.049219	-0.044167
0.000613	0.003640	0.036928	-0.003036	0.049283	-0.044530
0.000792	0.004034	0.037974	-0.005007	0.049343	-0.044863
0.001003	0.004454	0.038945	-0.006996	0.049398	-0.045170
0.001248	0.004900	0.039844	-0.008990	0.049448	-0.045453
0.001531	0.005373	0.040675	-0.010975	0.049494	-0.045713
0.001856	0.005872	0.041441	-0.012942	0.049536	-0.045951
0.002226	0.006396	0.042145	-0.014877	0.049575	-0.046170
0.002647	0.006946	0.042792	-0.016775	0.049611	-0.046371
0.003124	0.007519	0.043386	-0.018625	0.049644	-0.046556
0.003664	0.008114	0.043931	-0.020421	0.049674	-0.046726
0.004270	0.008725	0.044430	-0.022159	0.049701	-0.046882
0.004952	0.009348	0.044887	-0.023831	0.049716	-0.047025
0.005715	0.009977	0.045307	-0.025437	0.049684	-0.047153
0.006568	0.010603	0.045691	-0.026972	0.049616	-0.047254
0.007515	0.011213	0.046042	-0.028435	0.049528	-0.047322
0.008565	0.011794	0.046365	-0.029826	0.049433	-0.047358
0.009723	0.012326	0.046661	-0.031143		

101 nr of points on pressure side

0.000247	0.000000	0.014028	0.000125	0.045516	-0.036069
0.000287	-0.000076	0.015143	-0.000036	0.045826	-0.036969
0.000334	-0.000154	0.016308	-0.000263	0.046109	-0.037806
0.000388	-0.000234	0.017519	-0.000564	0.046373	-0.038597
0.000451	-0.000314	0.018771	-0.000945	0.046618	-0.039343
0.000524	-0.000395	0.020055	-0.001414	0.046842	-0.040032
0.000617	-0.000481	0.021365	-0.001975	0.047049	-0.040678
0.000725	-0.000563	0.022690	-0.002634	0.047241	-0.041282
0.000851	-0.000638	0.024022	-0.003390	0.047418	-0.041848
0.000995	-0.000705	0.025351	-0.004246	0.047580	-0.042366
0.001162	-0.000761	0.026668	-0.005197	0.047729	-0.042848
0.001347	-0.000803	0.027964	-0.006241	0.047866	-0.043296
0.001552	-0.000831	0.029230	-0.007370	0.047993	-0.043713
0.001780	-0.000844	0.030461	-0.008579	0.048110	-0.044099
0.002023	-0.000842	0.031651	-0.009857	0.048218	-0.044457
0.002294	-0.000826	0.032794	-0.011195	0.048316	-0.044782
0.002579	-0.000798	0.033887	-0.012583	0.048405	-0.045082
0.002896	-0.000755	0.034929	-0.014009	0.048488	-0.045359
0.003230	-0.000703	0.035919	-0.015465	0.048563	-0.045615
0.003597	-0.000638	0.036856	-0.016938	0.048633	-0.045851
0.003991	-0.000564	0.037740	-0.018421	0.048697	-0.046069
0.004417	-0.000481	0.038574	-0.019905	0.048756	-0.046269
0.004881	-0.000391	0.039354	-0.021371	0.048810	-0.046453
0.005374	-0.000297	0.040085	-0.022819	0.048859	-0.046623
0.005915	-0.000198	0.040771	-0.024245	0.048905	-0.046778
0.006495	-0.000099	0.041414	-0.025641	0.048946	-0.046921
0.007118	-0.000002	0.042010	-0.026991	0.048984	-0.047053
0.007793	0.000089	0.042568	-0.028304	0.049026	-0.047171
0.008521	0.000170	0.043088	-0.029570	0.049093	-0.047262
0.009295	0.000235	0.043570	-0.030785	0.049177	-0.047324
0.010127	0.000281	0.044021	-0.031952	0.049267	-0.047358
0.011016	0.000300	0.044437	-0.033060	0.049354	-0.047368
0.011963	0.000285	0.044825	-0.034120	0.049433	-0.047358
0.012967	0.000230	0.045184	-0.035122		

The turbine stator blade coordinates are listed in following table
(x and R*theta in m) located at Midsection (R= 0.84)

101 number of points on the suction side

0.000247	0.000000	0.010991	0.012790	0.046933	-0.032388
0.000203	0.000091	0.012369	0.013160	0.047182	-0.033562
0.000160	0.000194	0.013852	0.013410	0.047411	-0.034665
0.000120	0.000309	0.015431	0.013513	0.047621	-0.035701
0.000084	0.000436	0.017088	0.013445	0.047815	-0.036672
0.000052	0.000577	0.018802	0.013186	0.047993	-0.037578
0.000026	0.000733	0.020550	0.012726	0.048156	-0.038424
0.000009	0.000903	0.022303	0.012062	0.048307	-0.039212
0.000000	0.001092	0.024043	0.011196	0.048445	-0.039945
0.000003	0.001294	0.025747	0.010141	0.048572	-0.040626
0.000018	0.001516	0.027400	0.008912	0.048689	-0.041257
0.000047	0.001759	0.028991	0.007526	0.048797	-0.041842
0.000091	0.002017	0.030509	0.006003	0.048896	-0.042383
0.000153	0.002297	0.031953	0.004360	0.048987	-0.042885
0.000234	0.002599	0.033317	0.002617	0.049071	-0.043347
0.000336	0.002923	0.034601	0.000791	0.049148	-0.043773
0.000462	0.003270	0.035804	-0.001098	0.049219	-0.044167
0.000613	0.003640	0.036928	-0.003036	0.049283	-0.044530
0.000792	0.004034	0.037974	-0.005007	0.049343	-0.044863
0.001003	0.004454	0.038945	-0.006996	0.049398	-0.045170
0.001248	0.004900	0.039844	-0.008990	0.049448	-0.045453
0.001531	0.005373	0.040675	-0.010975	0.049494	-0.045713
0.001856	0.005872	0.041441	-0.012942	0.049536	-0.045951
0.002226	0.006396	0.042145	-0.014877	0.049575	-0.046170
0.002647	0.006946	0.042792	-0.016775	0.049611	-0.046371
0.003124	0.007519	0.043386	-0.018625	0.049644	-0.046556
0.003664	0.008114	0.043931	-0.020421	0.049674	-0.046726
0.004270	0.008725	0.044430	-0.022159	0.049701	-0.046882
0.004952	0.009348	0.044887	-0.023831	0.049716	-0.047025
0.005715	0.009977	0.045307	-0.025437	0.049684	-0.047153
0.006568	0.010603	0.045691	-0.026972	0.049616	-0.047254
0.007515	0.011213	0.046042	-0.028435	0.049528	-0.047322
0.008565	0.011794	0.046365	-0.029826	0.049433	-0.047358
0.009723	0.012326	0.046661	-0.031143		

101 number of points on the pressure side

0.000247	0.000000
0.000287	-0.000076
0.000334	-0.000154
0.000388	-0.000234
0.000451	-0.000314
0.000524	-0.000395
0.000617	-0.000481
0.000725	-0.000563
0.000851	-0.000638
0.000995	-0.000705
0.001162	-0.000761
0.001347	-0.000803
0.001552	-0.000831
0.001780	-0.000844
0.002023	-0.000842
0.002294	-0.000826
0.002579	-0.000798
0.002896	-0.000755
0.003230	-0.000703
0.003597	-0.000638
0.003991	-0.000564
0.004417	-0.000481
0.004881	-0.000391
0.005374	-0.000297
0.005915	-0.000198
0.006495	-0.000099
0.007118	-0.000002
0.007793	0.000089
0.008521	0.000170
0.009295	0.000235
0.010127	0.000281
0.011016	0.000300
0.011963	0.000285
0.012967	0.000230
0.014028	0.000125
0.015143	-0.000036
0.016308	-0.000263
0.017519	-0.000564
0.018771	-0.000945
0.020055	-0.001414
0.021365	-0.001975
0.022690	-0.002634
0.024022	-0.003390
0.025351	-0.004246
0.026668	-0.005197
0.027964	-0.006241
0.029230	-0.007370
0.030461	-0.008579
0.031651	-0.009857
0.032794	-0.011195
0.033887	-0.012583
0.034929	-0.014009
0.035919	-0.015465
0.036856	-0.016938
0.037740	-0.018421
0.038574	-0.019905
0.039354	-0.021371
0.040085	-0.022819
0.040771	-0.024245
0.041414	-0.025641
0.042010	-0.026991
0.042568	-0.028304
0.043088	-0.029570
0.043570	-0.030785
0.044021	-0.031952
0.044437	-0.033060
0.044825	-0.034120
0.045184	-0.035122
0.045516	-0.036069
0.045826	-0.036969
0.046109	-0.037806
0.046373	-0.038597
0.046618	-0.039343
0.046842	-0.040032
0.047049	-0.040678
0.047241	-0.041282
0.047418	-0.041848
0.047580	-0.042366
0.047729	-0.042848
0.047866	-0.043296
0.047993	-0.043713
0.048110	-0.044099
0.048218	-0.044457
0.048316	-0.044782
0.048405	-0.045082
0.048488	-0.045359
0.048563	-0.045615
0.048633	-0.045851
0.048697	-0.046069
0.048756	-0.046269
0.048810	-0.046453
0.048859	-0.046623
0.048905	-0.046778
0.048946	-0.046921
0.048984	-0.047053
0.049026	-0.047171
0.049093	-0.047262
0.049177	-0.047324
0.049267	-0.047358
0.049354	-0.047368
0.049433	-0.047358

The turbine stator blade coordinates are listed in following table
(x and R*theta in m) located at shroud (R= 0.904)

101 number of points on the suction side

0.000247	0.000000
0.000203	0.000091
0.000160	0.000194
0.000120	0.000309
0.000084	0.000436
0.000052	0.000577
0.000026	0.000733
0.000009	0.000903
0.000000	0.001092
0.000003	0.001294
0.000018	0.001516
0.000047	0.001759
0.000091	0.002017
0.000153	0.002297
0.000234	0.002599
0.000336	0.002923
0.000462	0.003270
0.000613	0.003640
0.000792	0.004034
0.001003	0.004454
0.001248	0.004900
0.001531	0.005373
0.001856	0.005872
0.002226	0.006396
0.002647	0.006946
0.003124	0.007519
0.003664	0.008114
0.004270	0.008725
0.004952	0.009348
0.005715	0.009977
0.006568	0.010603
0.007515	0.011213
0.008565	0.011794
0.009723	0.012326
0.010991	0.012790
0.012369	0.013160
0.013852	0.013410
0.015431	0.013513
0.017088	0.013445
0.018802	0.013186
0.020550	0.012726
0.022303	0.012062
0.024043	0.011196
0.025747	0.010141
0.027400	0.008912
0.028991	0.007526
0.030509	0.006003
0.031953	0.004360
0.033317	0.002617
0.034601	0.000791
0.035804	-0.001098
0.036928	-0.003036
0.037974	-0.005007
0.038945	-0.006996
0.039844	-0.008990
0.040675	-0.010975
0.041441	-0.012942
0.042145	-0.014877
0.042792	-0.016775
0.043386	-0.018625
0.043931	-0.020421
0.044430	-0.022159
0.044887	-0.023831
0.045307	-0.025437
0.045691	-0.026972
0.046042	-0.028435
0.046365	-0.029826
0.046661	-0.031143
0.046933	-0.032388
0.047182	-0.033562
0.047411	-0.034665
0.047621	-0.035701
0.047815	-0.036672
0.047993	-0.037578
0.048156	-0.038424
0.048307	-0.039212
0.048445	-0.039945
0.048572	-0.040626
0.048689	-0.041257
0.048797	-0.041842
0.048896	-0.042383
0.048987	-0.042885
0.049071	-0.043347
0.049148	-0.043773
0.049219	-0.044167
0.049283	-0.044530
0.049343	-0.044863
0.049398	-0.045170
0.049448	-0.045453
0.049494	-0.045713
0.049536	-0.045951
0.049575	-0.046170
0.049611	-0.046371
0.049644	-0.046556
0.049674	-0.046726
0.049701	-0.046882
0.049716	-0.047025
0.049684	-0.047153
0.049616	-0.047254
0.049528	-0.047322
0.049433	-0.047358

101 number of points on the pressure side

0.000247	0.000000
0.000287	-0.000076
0.000334	-0.000154
0.000388	-0.000234
0.000451	-0.000314
0.000524	-0.000395
0.000617	-0.000481
0.000725	-0.000563
0.000851	-0.000638
0.000995	-0.000705
0.001162	-0.000761
0.001347	-0.000803
0.001552	-0.000831
0.001780	-0.000844
0.002023	-0.000842
0.002294	-0.000826
0.002579	-0.000798
0.002896	-0.000755
0.003230	-0.000703
0.003597	-0.000638
0.003991	-0.000564
0.004417	-0.000481
0.004881	-0.000391
0.005374	-0.000297
0.005915	-0.000198
0.006495	-0.000099
0.007118	-0.000002
0.007793	0.000089
0.008521	0.000170
0.009295	0.000235
0.010127	0.000281
0.011016	0.000300
0.011963	0.000285
0.012967	0.000230
0.014028	0.000125
0.015143	-0.000036
0.016308	-0.000263
0.017519	-0.000564
0.018771	-0.000945
0.020055	-0.001414
0.021365	-0.001975
0.022690	-0.002634
0.024022	-0.003390
0.025351	-0.004246
0.026668	-0.005197
0.027964	-0.006241
0.029230	-0.007370
0.030461	-0.008579
0.031651	-0.009857
0.032794	-0.011195
0.033887	-0.012583
0.034929	-0.014009
0.035919	-0.015465
0.036856	-0.016938
0.037740	-0.018421
0.038574	-0.019905
0.039354	-0.021371
0.040085	-0.022819
0.040771	-0.024245
0.041414	-0.025641
0.042010	-0.026991
0.042568	-0.028304
0.043088	-0.029570
0.043570	-0.030785
0.044021	-0.031952
0.044437	-0.033060
0.044825	-0.034120
0.045184	-0.035122
0.045516	-0.036069
0.045826	-0.036969
0.046109	-0.037806
0.046373	-0.038597
0.046618	-0.039343
0.046842	-0.040032
0.047049	-0.040678
0.047241	-0.041282
0.047418	-0.041848
0.047580	-0.042366
0.047729	-0.042848
0.047866	-0.043296
0.047993	-0.043713
0.048110	-0.044099
0.048218	-0.044457
0.048316	-0.044782
0.048405	-0.045082
0.048488	-0.045359
0.048563	-0.045615
0.048633	-0.045851
0.048697	-0.046069
0.048756	-0.046269
0.048810	-0.046453
0.048859	-0.046623
0.048905	-0.046778
0.048946	-0.046921
0.048984	-0.047053
0.049026	-0.047171
0.049093	-0.047262
0.049177	-0.047324
0.049267	-0.047358
0.049354	-0.047368
0.049433	-0.047358

The turbine rotor blade coordinates are listed in following table
(x and R*theta in m) located at hub (R= 0.78)

101 number of points on the pressure side

-0.02088479	0.004103039
-0.02085079	0.004159039
-0.02081179	0.004216039
-0.02076779	0.004273039
-0.02071779	0.004330039
-0.02065779	0.004387039
-0.02058279	0.004446039
-0.02049679	0.004499039
-0.02039679	0.004546039
-0.02028379	0.004583039
-0.02015179	0.004609039
-0.02001279	0.004622039
-0.01985479	0.004622039
-0.01968579	0.004609039
-0.01950279	0.004582039
-0.01930479	0.004543039
-0.01909379	0.004492039
-0.01886379	0.004428039
-0.01861879	0.004354039
-0.01835279	0.004268039
-0.01806579	0.004172039
-0.01775879	0.004066039
-0.01742079	0.003948039
-0.01706579	0.003824039
-0.01667479	0.003690039
-0.01625479	0.003550039
-0.01580379	0.003405039
-0.01531379	0.003254039
-0.01478479	0.003101039
-0.01422079	0.002950039
-0.01361279	0.002801039
-0.01295879	0.002658039
-0.01225879	0.002524039
-0.01151079	0.002404039
-0.01071679	0.002301039
-0.00987479	0.002221039
-0.00898379	0.002169039
-0.00804579	0.002149039
-0.00706179	0.002167039
-0.00603479	0.002229039
-0.00496779	0.002340039
-0.00386679	0.002505039
-0.00273479	0.002729039
-0.00158079	0.003015039
-0.00041179	0.003367039
0.00076721	0.003786039
0.00194621	0.004273039
0.00311721	0.004829039
0.00427421	0.005449039
0.00540721	0.006132039
0.00651121	0.006872039
0.00757921	0.007662039
0.00860621	0.008497039
0.00958921	0.009367039
0.01052621	0.010266039
0.01141521	0.011186039
0.01225121	0.012113039
0.01303921	0.013044039
0.01378021	0.013974039
0.01447721	0.014898039
0.01512421	0.015799039
0.01573021	0.016683039
0.01629821	0.017546039
0.01682321	0.018372039
0.01731621	0.019177039
0.01777021	0.019940039
0.01819821	0.020677039
0.01859021	0.021369039
0.01895721	0.022032039
0.01929821	0.022657039
0.01961321	0.023245039
0.01990721	0.023801039
0.02017921	0.024321039
0.02043021	0.024806039
0.02066421	0.025261039
0.02088121	0.025688039
0.02108121	0.026081039
0.02126521	0.026446039
0.02143521	0.026787039
0.02159421	0.027103039
0.02174021	0.027397039
0.02187521	0.027669039
0.02199821	0.027916039
0.02211221	0.028146039
0.02221721	0.028358039
0.02231321	0.028554039
0.02240321	0.028734039
0.02248521	0.028901039
0.02256121	0.029054039
0.02263021	0.029195039
0.02269421	0.029325039
0.02275321	0.029444039
0.02281921	0.029546039
0.02289821	0.029624039
0.02298221	0.029681039
0.02306821	0.029718039
0.02315221	0.029739039
0.02323021	0.029746039
0.02330221	0.029743039
0.02336721	0.029731039
0.02342521	0.029714039

101 number of points on the suction side

-0.02088479	0.004103039
-0.02092479	0.004029039
-0.02096379	0.003943039
-0.02100079	0.003850039
-0.02103579	0.003743039
-0.02106679	0.003628039
-0.02109479	0.003497039
-0.02111679	0.003356039
-0.02113379	0.003200039
-0.02114579	0.003027039
-0.02114979	0.002842039
-0.02114679	0.002639039
-0.02113579	0.002418039
-0.02111579	0.002177039
-0.02108679	0.001918039
-0.02104679	0.001637039
-0.02099479	0.001333039
-0.02092879	0.001004039
-0.02084979	0.000648039
-0.02075379	0.000266039
-0.02063979	-0.000144961
-0.02050579	-0.000586961
-0.02034879	-0.001059961
-0.02016679	-0.001566961
-0.01995579	-0.002107961
-0.01971279	-0.002683961
-0.01943279	-0.003296961
-0.01911379	-0.003943961
-0.01874679	-0.004625961
-0.01832779	-0.005342961
-0.01785079	-0.006088961
-0.01730879	-0.006862961
-0.01669179	-0.007657961
-0.01599479	-0.008466961
-0.01520579	-0.009279961
-0.01431879	-0.010082961
-0.01332579	-0.010859961
-0.01221779	-0.011590961
-0.01099379	-0.012249961
-0.00965279	-0.012810961
-0.00820079	-0.013241961
-0.00665179	-0.013513961
-0.00502579	-0.013598961
-0.00335079	-0.013475961
-0.00165779	-0.013134961
1.92E-05	-0.012578961
0.00165521	-0.011817961
0.00322521	-0.010874961
0.00471821	-0.009770961
0.00612021	-0.008533961
0.00743121	-0.007190961
0.00865221	-0.005762961
0.00978521	-0.004273961
0.01083521	-0.002743961
0.01180721	-0.001188961
0.01270721	0.000375039
0.01354221	0.001935039
0.01431621	0.003479039
0.01503621	0.004997039
0.01570721	0.006483039
0.01633221	0.007927039
0.01691621	0.009325039
0.01746221	0.010673039
0.01797421	0.011967039
0.01845321	0.013204039
0.01890321	0.014383039
0.01932321	0.015503039
0.01971721	0.016565039
0.02008421	0.017568039
0.02042721	0.018514039
0.02074621	0.019403039
0.02104321	0.020238039
0.02131721	0.021021039
0.02157021	0.021753039
0.02180321	0.022437039
0.02201721	0.023074039
0.02221321	0.023668039
0.02239321	0.024220039
0.02255621	0.024733039
0.02270421	0.025209039
0.02283921	0.025650039
0.02296221	0.026059039
0.02307321	0.026437039
0.02317321	0.026786039
0.02326421	0.027109039
0.02334521	0.027406039
0.02341921	0.027681039
0.02348621	0.027934039
0.02354721	0.028167039
0.02360121	0.028381039
0.02365021	0.028578039
0.02369521	0.028759039
0.02373521	0.028926039
0.02377221	0.029080039
0.02378521	0.029223039
0.02376421	0.029354039
0.02371721	0.029465039
0.02365421	0.029557039
0.02358021	0.029627039
0.02350321	0.029679039
0.02342521	0.029714039

The turbine rotor blade coordinates are listed in following table
(x and R*theta in m) located at shroud (R= 0.90)

101 number of points on the pressure side

-0.01814955	0.00195992
-0.01813055	0.00201892
-0.01810755	0.00207992
-0.01807755	0.00214192
-0.01804155	0.00220392
-0.01799155	0.00227092
-0.01792955	0.00233592
-0.01785255	0.00239692
-0.01776355	0.00244992
-0.01765455	0.00249792
-0.01753555	0.00253392
-0.01740055	0.00256192
-0.01725055	0.00257992
-0.01708855	0.00258792
-0.01690755	0.00258592
-0.01671755	0.00257592
-0.01650455	0.00255592
-0.01628255	0.00252792
-0.01603355	0.00249092
-0.01577255	0.00244692
-0.01548555	0.00239292
-0.01517855	0.00233292
-0.01484655	0.00226392
-0.01448455	0.00218792
-0.01410155	0.00210592
-0.01368355	0.00201592
-0.01323555	0.00192192
-0.01275555	0.00182492
-0.01223755	0.00172292
-0.01168055	0.00162092
-0.01108855	0.00151892
-0.01045355	0.00142092
-0.00977455	0.00132792
-0.00905155	0.00124392
-0.00828355	0.00117292
-0.00747255	0.00111892
-0.00661555	0.00108592
-0.00571255	0.00107992
-0.00476655	0.00110492
-0.00377955	0.00116792
-0.00275455	0.00127392
-0.00169455	0.00142992
-0.00060655	0.00164092
0.00050445	0.00191292
0.00163045	0.00224892
0.00276445	0.00265492
0.00389545	0.00313092
0.00501545	0.00367792
0.00611645	0.00429592
0.00718845	0.00497992
0.00822445	0.00572692
0.00921845	0.00653092
0.01016445	0.00738292
0.01105845	0.00827492
0.01189845	0.00919792
0.01268045	0.01014092
0.01340945	0.01109592
0.01408445	0.01205692
0.01470945	0.01301692
0.01528445	0.01396592
0.01581145	0.01489392
0.01629745	0.01580492
0.01674345	0.01668892
0.01715045	0.01754092
0.01752745	0.01836492
0.01786945	0.01914792
0.01818645	0.01990192
0.01847445	0.02061292
0.01874145	0.02128992
0.01898645	0.02193092
0.01921045	0.02253092
0.01941745	0.02309892
0.01960845	0.02363092
0.01978345	0.02412592
0.01994545	0.02458992
0.02009545	0.02502492
0.02023245	0.02542692
0.02035945	0.02579992
0.02047545	0.02614692
0.02058345	0.02646892
0.02068345	0.02676792
0.02077445	0.02704392
0.02085845	0.02729792
0.02093645	0.02753192
0.02100745	0.02774892
0.02107345	0.02794792
0.02113345	0.02813192
0.02118945	0.02830192
0.02124045	0.02845792
0.02128745	0.02860092
0.02133145	0.02873192
0.02138845	0.02884592
0.02146045	0.02893692
0.02154145	0.02900692
0.02162545	0.02905792
0.02170845	0.02909092
0.02178945	0.02911092
0.02186445	0.02911792
0.02193345	0.02911692
0.02199645	0.02910892
0.02205345	0.02909492

101 number of points on the suction side

-0.01814955	0.00195992
-0.01816555	0.00189292
-0.01818155	0.00180892
-0.01819455	0.00171992
-0.01820655	0.00162292
-0.01821655	0.00151192
-0.01822355	0.00139792
-0.01822955	0.00126692
-0.01823255	0.00112992
-0.01823355	0.00097592
-0.01823055	0.00081092
-0.01822455	0.00062992
-0.01821355	0.00043492
-0.01819855	0.00021992
-0.01817655	-0.00001008
-0.01814755	-0.00026208
-0.01811055	-0.00053308
-0.01806355	-0.00082708
-0.01800455	-0.00114408
-0.01793155	-0.00148708
-0.01784155	-0.00185508
-0.01773055	-0.00224908
-0.01759655	-0.00267108
-0.01743455	-0.00312108
-0.01723955	-0.00359808
-0.01700455	-0.00410108
-0.01672555	-0.00462908
-0.01639455	-0.00517808
-0.01600555	-0.00574408
-0.01555155	-0.00632308
-0.01502655	-0.00690908
-0.01442455	-0.00749308
-0.01374155	-0.00806708
-0.01297455	-0.00862408
-0.01211955	-0.00915208
-0.01117655	-0.00964008
-0.01014555	-0.01007608
-0.00902755	-0.01044508
-0.00782655	-0.01072908
-0.00654855	-0.01091008
-0.00520555	-0.01096608
-0.00381255	-0.01088108
-0.00238755	-0.01063708
-0.00095355	-0.01022808
0.00046745	-0.00965508
0.00185845	-0.00892608
0.00320145	-0.00805808
0.00449345	-0.00706608
0.00572345	-0.00597408
0.00689545	-0.00479708
0.00800645	-0.00355408
0.00905845	-0.00226008
0.01005345	-0.00093108
0.01099345	0.00042192
0.01187945	0.00178692
0.01271345	0.00315392
0.01349745	0.00451292
0.01423345	0.00585792
0.01492245	0.00718192
0.01556545	0.00847692
0.01616345	0.00973892
0.01671845	0.01096392
0.01723345	0.01214792
0.01770845	0.01328792
0.01814545	0.01438092
0.01854745	0.01542592
0.01891645	0.01642192
0.01925445	0.01736792
0.01956345	0.01826492
0.01984545	0.01911192
0.02010345	0.01990992
0.02033945	0.02065992
0.02055445	0.02136392
0.02075145	0.02202292
0.02093045	0.02263792
0.02109445	0.02321192
0.02124445	0.02374692
0.02138145	0.02424292
0.02150745	0.02470492
0.02162145	0.02513192
0.02172745	0.02552792
0.02182345	0.02589392
0.02191245	0.02623192
0.02199345	0.02654492
0.02206745	0.02683292
0.02213645	0.02709792
0.02219845	0.02734292
0.02225645	0.02756792
0.02230945	0.02777492
0.02235745	0.02796492
0.02240145	0.02813992
0.02244245	0.02829992
0.02247545	0.02844892
0.02247745	0.02858792
0.02245045	0.02871292
0.02240245	0.02881992
0.02234045	0.02890792
0.02227145	0.02897792
0.02219845	0.02903092
0.02212445	0.02906992
0.02205345	0.02909492

Appendix II Coordinates of the optimized compressor stator and rotor

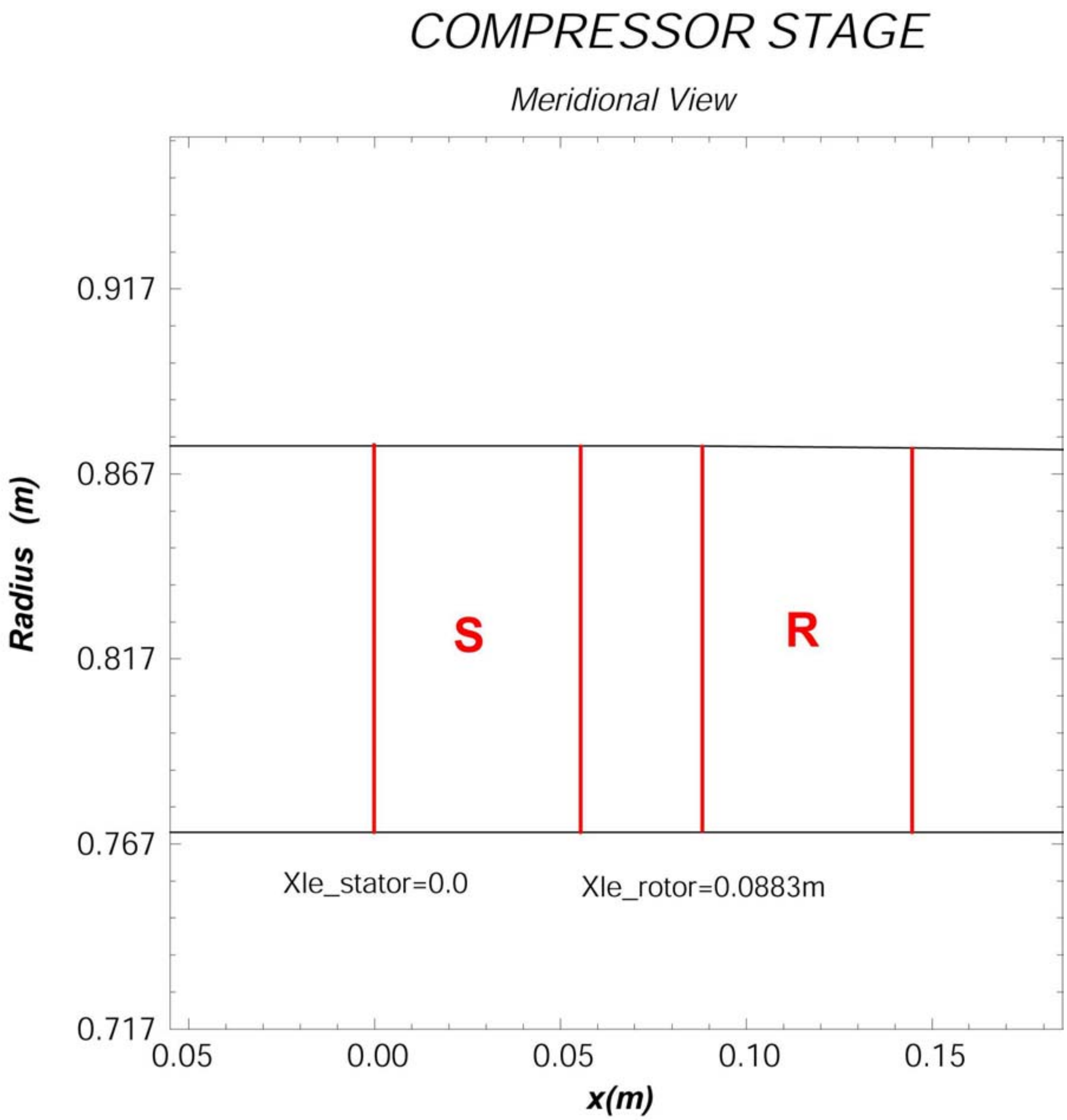

The compressor hub and shroud coordinates x and R (m) are listed in following table. Xle_stator and Xle_rotor are the position of the stator and rotor leading at the hub

x(hub)	R(hub)	X(shroud)	R(shroud)
-0.23714	0.770207	-0.23259	0.874575
-0.172957	0.770207	-0.172957	0.874575
-0.108772	0.770207	-0.108772	0.874575
-0.0445882	0.770207	-0.0445882	0.874575
0.0195955	0.770207	0.0832336	0.874575
0.0837796	0.770207	0.0837796	0.87457
0.147963	0.770207	0.147963	0.873981
0.212147	0.770207	0.212147	0.873293
0.276332	0.770207	0.276332	0.872705
0.340515	0.770207	0.340515	0.872116
0.404699	0.770207	0.404699	0.871528
0.468883	0.770207	0.468883	0.870845
0.533067	0.770207	0.533067	0.870257
0.597251	0.770207	0.597251	0.869668
0.661433	0.770207	0.661433	0.868981
0.725621	0.770207	0.725621	0.868392

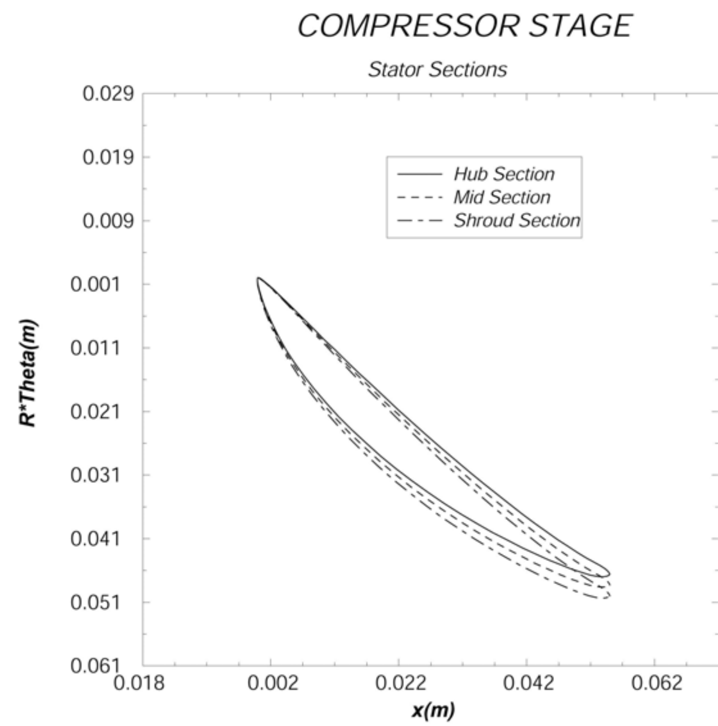

Compressor stator blade sections

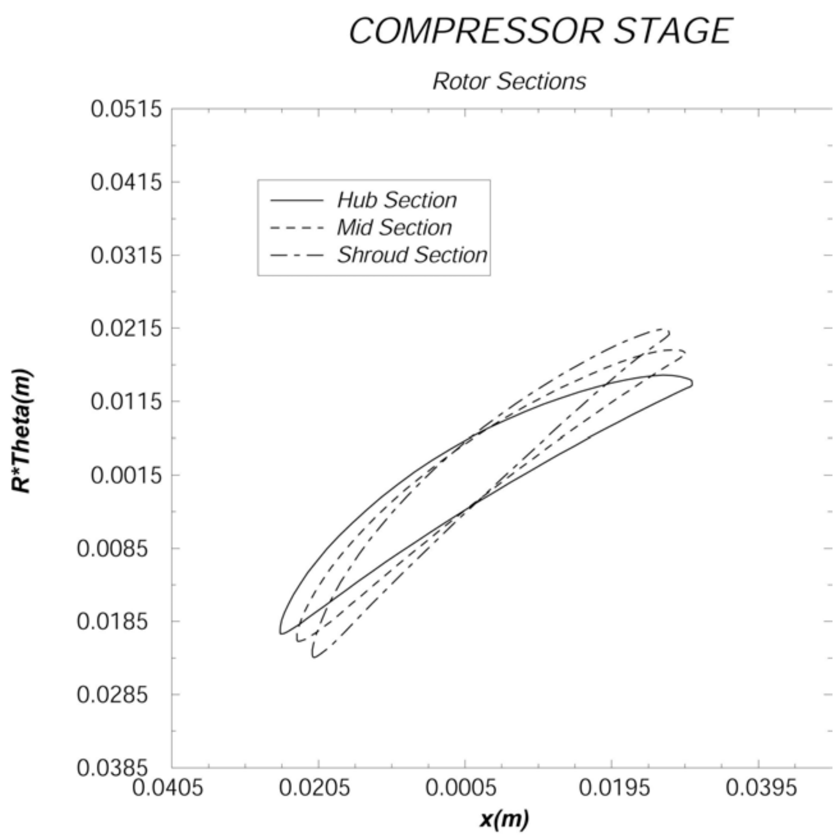

Compressor rotor blade sections

The compressor stator blade coordinates are listed in following table
(x and R*theta in m) located at Hub (R=0. 0.7860)

39 nr of points on pressure side

-0.00002000	0.00003000
0.00014000	0.00002000
0.00047000	-0.00014000
0.00098000	-0.00052000
0.00166000	-0.00110000
0.00249000	-0.00185000
0.00348000	-0.00279000
0.00460000	-0.00389000
0.00586000	-0.00515000
0.00724000	-0.00654000
0.00875000	-0.00806000
0.01037000	-0.00968000
0.01211000	-0.01139000
0.01394000	-0.01317000
0.01585000	-0.01502000
0.01784000	-0.01691000
0.01990000	-0.01883000
0.02201000	-0.02078000
0.02415000	-0.02273000
0.02633000	-0.02468000
0.02852000	-0.02661000
0.03072000	-0.02851000
0.03290000	-0.03036000
0.03507000	-0.03216000
0.03720000	-0.03389000
0.03928000	-0.03554000
0.04131000	-0.03711000
0.04325000	-0.03857000
0.04511000	-0.03991000
0.04686000	-0.04114000
0.04849000	-0.04224000
0.04998000	-0.04321000
0.05133000	-0.04402000
0.05251000	-0.04470000
0.05349000	-0.04525000
0.05424000	-0.04572000
0.05472000	-0.04614000
0.05495000	-0.04643000
0.05501000	-0.04658000

39 nr of points on suction side

-0.00002000	0.00003000
-0.00009000	-0.00012000
-0.00010000	-0.00048000
0.00000000	-0.00111000
0.00022000	-0.00198000
0.00055000	-0.00307000
0.00101000	-0.00437000
0.00162000	-0.00585000
0.00238000	-0.00751000
0.00330000	-0.00931000
0.00439000	-0.01124000
0.00567000	-0.01326000
0.00714000	-0.01534000
0.00879000	-0.01747000
0.01061000	-0.01962000
0.01258000	-0.02177000
0.01469000	-0.02390000
0.01693000	-0.02600000
0.01926000	-0.02806000
0.02168000	-0.03005000
0.02415000	-0.03196000
0.02667000	-0.03378000
0.02921000	-0.03551000
0.03174000	-0.03712000
0.03424000	-0.03862000
0.03669000	-0.04001000
0.03907000	-0.04128000
0.04134000	-0.04243000
0.04350000	-0.04346000
0.04553000	-0.04436000
0.04740000	-0.04514000
0.04910000	-0.04579000
0.05061000	-0.04631000
0.05193000	-0.04671000
0.05305000	-0.04694000
0.05394000	-0.04698000
0.05456000	-0.04686000
0.05490000	-0.04670000
0.05501000	-0.04658000

The compressor stator blade coordinates are listed in following table
(x and R*theta in m) located at Midsection (R=0. 0.8392500)

39 nr of points on pressure side

-0.00001000	0.00002000
0.00015000	0.00000000
0.00048000	-0.00018000
0.00100000	-0.00057000
0.00167000	-0.00117000
0.00251000	-0.00195000
0.00349000	-0.00292000
0.00461000	-0.00406000
0.00587000	-0.00535000
0.00724000	-0.00679000
0.00875000	-0.00836000
0.01037000	-0.01003000
0.01209000	-0.01180000
0.01392000	-0.01364000
0.01583000	-0.01555000
0.01782000	-0.01750000
0.01987000	-0.01949000
0.02197000	-0.02150000
0.02411000	-0.02352000
0.02629000	-0.02553000
0.02848000	-0.02753000
0.03067000	-0.02949000
0.03285000	-0.03141000
0.03502000	-0.03328000
0.03715000	-0.03507000
0.03924000	-0.03678000
0.04126000	-0.03840000
0.04321000	-0.03992000
0.04507000	-0.04132000
0.04682000	-0.04260000
0.04846000	-0.04374000
0.04996000	-0.04475000
0.05131000	-0.04560000
0.05249000	-0.04630000
0.05348000	-0.04688000
0.05422000	-0.04739000
0.05471000	-0.04782000
0.05495000	-0.04811000
0.05500000	-0.04826000

39 nr of points on suction side

-0.00001000	0.00002000
-0.00007000	-0.00013000
-0.00008000	-0.00051000
0.00000000	-0.00115000
0.00020000	-0.00204000
0.00052000	-0.00315000
0.00097000	-0.00447000
0.00156000	-0.00599000
0.00229000	-0.00768000
0.00320000	-0.00953000
0.00427000	-0.01150000
0.00554000	-0.01357000
0.00699000	-0.01571000
0.00862000	-0.01790000
0.01043000	-0.02011000
0.01239000	-0.02233000
0.01450000	-0.02453000
0.01672000	-0.02671000
0.01906000	-0.02883000
0.02147000	-0.03089000
0.02395000	-0.03288000
0.02648000	-0.03477000
0.02902000	-0.03656000
0.03156000	-0.03825000
0.03407000	-0.03982000
0.03653000	-0.04127000
0.03892000	-0.04260000
0.04120000	-0.04380000
0.04338000	-0.04488000
0.04541000	-0.04583000
0.04730000	-0.04665000
0.04901000	-0.04735000
0.05054000	-0.04791000
0.05187000	-0.04833000
0.05300000	-0.04857000
0.05390000	-0.04862000
0.05454000	-0.04852000
0.05489000	-0.04837000
0.05500000	-0.04826000

The compressor stator blade coordinates are listed in following table
(x and R*theta in m) located at shroud (R=0. 0.8925000)

39 nr of points on pressure side

-0.00001000	0.00002000
0.00015000	-0.00001000
0.00048000	-0.00020000
0.00100000	-0.00060000
0.00168000	-0.00122000
0.00251000	-0.00203000
0.00349000	-0.00303000
0.00461000	-0.00420000
0.00586000	-0.00554000
0.00724000	-0.00703000
0.00873000	-0.00865000
0.01035000	-0.01037000
0.01207000	-0.01220000
0.01389000	-0.01410000
0.01580000	-0.01607000
0.01778000	-0.01809000
0.01983000	-0.02014000
0.02193000	-0.02222000
0.02407000	-0.02431000
0.02624000	-0.02639000
0.02843000	-0.02846000
0.03062000	-0.03049000
0.03281000	-0.03248000
0.03497000	-0.03442000
0.03711000	-0.03628000
0.03920000	-0.03805000
0.04122000	-0.03973000
0.04318000	-0.04131000
0.04504000	-0.04276000
0.04680000	-0.04409000
0.04844000	-0.04528000
0.04994000	-0.04633000
0.05130000	-0.04721000
0.05249000	-0.04795000
0.05348000	-0.04856000
0.05423000	-0.04909000
0.05471000	-0.04953000
0.05495000	-0.04983000
0.05500000	-0.04998000

39 number of points on suction side

-0.00001000	0.00002000
-0.00007000	-0.00013000
-0.00009000	-0.00051000
-0.00002000	-0.00117000
0.00017000	-0.00207000
0.00047000	-0.00321000
0.00090000	-0.00456000
0.00147000	-0.00611000
0.00219000	-0.00784000
0.00308000	-0.00973000
0.00414000	-0.01176000
0.00538000	-0.01388000
0.00682000	-0.01608000
0.00844000	-0.01833000
0.01024000	-0.02061000
0.01219000	-0.02290000
0.01429000	-0.02517000
0.01651000	-0.02742000
0.01884000	-0.02962000
0.02126000	-0.03176000
0.02374000	-0.03381000
0.02627000	-0.03578000
0.02882000	-0.03765000
0.03137000	-0.03940000
0.03389000	-0.04104000
0.03637000	-0.04256000
0.03877000	-0.04395000
0.04107000	-0.04521000
0.04326000	-0.04635000
0.04531000	-0.04735000
0.04721000	-0.04822000
0.04893000	-0.04895000
0.05047000	-0.04955000
0.05182000	-0.05000000
0.05296000	-0.05026000
0.05388000	-0.05034000
0.05453000	-0.05024000
0.05489000	-0.05010000
0.05500000	-0.04998000

The compressor rotor blade coordinates are listed in following table
(x and R*theta in m) located at Hub (R= 0.786000)

39 nr of points on pressure side

-0.02566285	-0.02020898
-0.02573285	-0.02006898
-0.02576285	-0.01973898
-0.02571285	-0.01913898
-0.02551285	-0.01832898
-0.02516285	-0.01733898
-0.02463285	-0.01616898
-0.02392285	-0.01485898
-0.02303285	-0.01341898
-0.02197285	-0.01186898
-0.02072285	-0.01022898
-0.01929285	-0.00852898
-0.01768285	-0.00679898
-0.01590285	-0.00502898
-0.01397285	-0.00326898
-0.01191285	-0.00150898
-0.00972285	0.00022102
-0.00742285	0.00190102
-0.00502285	0.00351102
-0.00254285	0.00504102
-0.00001285	0.00647102
0.00255715	0.00779102
0.00513715	0.00901102
0.00769715	0.01012102
0.01021715	0.01112102
0.01267715	0.01201102
0.01505715	0.01279102
0.01732715	0.01346102
0.01947715	0.01402102
0.02148715	0.01447102
0.02333715	0.01480102
0.02501715	0.01501102
0.02650715	0.01509102
0.02778715	0.01504102
0.02882715	0.01489102
0.02965715	0.01467102
0.03012715	0.01453102
0.03041715	0.01436102
0.03047715	0.01403102

39 nr. of points on the suction side

-0.02566285	-0.02020898
-0.02551285	-0.02021898
-0.02519285	-0.02014898
-0.02466285	-0.01989898
-0.02398285	-0.01947898
-0.02313285	-0.01889898
-0.02213285	-0.01817898
-0.02098285	-0.01733898
-0.01969285	-0.01638898
-0.01826285	-0.01533898
-0.01671285	-0.01419898
-0.01504285	-0.01298898
-0.01326285	-0.01171898
-0.01139285	-0.01040898
-0.00942285	-0.00906898
-0.00738285	-0.00769898
-0.00528285	-0.00631898
-0.00313285	-0.00493898
-0.00094285	-0.00354898
0.00126715	-0.00216898
0.00349715	-0.00080898
0.00572715	0.00052102
0.00794715	0.00183102
0.01013715	0.00310102
0.01229715	0.00432102
0.01439715	0.00548102
0.01646715	0.00661102
0.01852715	0.00770102
0.02050715	0.00874102
0.02233715	0.00968102
0.02401715	0.01053102
0.02553715	0.01128102
0.02687715	0.01194102
0.02802715	0.01250102
0.02897715	0.01295102
0.02974715	0.01331102
0.03019715	0.01351102
0.03045715	0.01370102
0.03047715	0.01403102

The compressor rotor blade coordinates are listed in following table
(x and R*theta in m) located at Midsection (R= 0.839550)

39 nr of points on pressure side

-0.02334799	-0.02120931	0.00055201	0.00648069
-0.02341799	-0.02107931	0.00294201	0.00802069
-0.02345799	-0.02074931	0.00533201	0.00948069
-0.02341799	-0.02016931	0.00772201	0.01084069
-0.02323799	-0.01936931	0.01007201	0.01210069
-0.02290799	-0.01837931	0.01237201	0.01326069
-0.02241799	-0.01721931	0.01460201	0.01432069
-0.02177799	-0.01589931	0.01673201	0.01527069
-0.02096799	-0.01444931	0.01874201	0.01611069
-0.01997799	-0.01287931	0.02064201	0.01684069
-0.01881799	-0.01120931	0.02239201	0.01745069
-0.01748799	-0.00947931	0.02398201	0.01793069
-0.01598799	-0.00769931	0.02541201	0.01826069
-0.01432799	-0.00587931	0.02666201	0.01845069
-0.01251799	-0.00403931	0.02769201	0.01853069
-0.01057799	-0.00220931	0.02852201	0.01851069
-0.00852799	-0.00037931	0.02909201	0.01841069
-0.00636799	0.00141069	0.02939201	0.01827069
-0.00411799	0.00316069	0.02949201	0.01816069
-0.00180799	0.00485069		

39 number of points on the suction side

-0.02334799	-0.02120931	0.00469201	0.00070069
-0.02319799	-0.02123931	0.00680201	0.00230069
-0.02287799	-0.02117931	0.00890201	0.00386069
-0.02233799	-0.02095931	0.01097201	0.00538069
-0.02162799	-0.02054931	0.01301201	0.00685069
-0.02076799	-0.01997931	0.01499201	0.00826069
-0.01976799	-0.01924931	0.01690201	0.00960069
-0.01862799	-0.01835931	0.01873201	0.01086069
-0.01737799	-0.01732931	0.02046201	0.01203069
-0.01601799	-0.01615931	0.02209201	0.01312069
-0.01452799	-0.01488931	0.02359201	0.01411069
-0.01293799	-0.01351931	0.02495201	0.01500069
-0.01124799	-0.01207931	0.02616201	0.01577069
-0.00945799	-0.01057931	0.02721201	0.01644069
-0.00759799	-0.00902931	0.02808201	0.01698069
-0.00565799	-0.00743931	0.02878201	0.01741069
-0.00365799	-0.00581931	0.02924201	0.01776069
-0.00160799	-0.00418931	0.02945201	0.01802069
0.00047201	-0.00254931	0.02949201	0.01816069
0.00257201	-0.00091931		

The compressor rotor blade coordinates are listed in following table
(x and R*theta in m) located at Shroud (R= 0.893100)

39 nr of points on pressure side

-0.02119236	-0.02342774
-0.02128236	-0.02329774
-0.02134236	-0.02297774
-0.02132236	-0.02239774
-0.02118236	-0.02159774
-0.02091236	-0.02059774
-0.02051236	-0.01940774
-0.01997236	-0.01804774
-0.01930236	-0.01653774
-0.01847236	-0.01488774
-0.01749236	-0.01313774
-0.01633236	-0.01128774
-0.01502236	-0.00937774
-0.01356236	-0.00741774
-0.01196236	-0.00541774
-0.01023236	-0.00339774
-0.00840236	-0.00136774
-0.00645236	0.00063226
-0.00442236	0.00260226
-0.00230236	0.00450226
-0.00012236	0.00633226
0.00209764	0.00808226
0.00434764	0.00974226
0.00658764	0.01130226
0.00879764	0.01277226
0.01095764	0.01414226
0.01305764	0.01540226
0.01507764	0.01655226
0.01698764	0.01759226
0.01877764	0.01851226
0.02043764	0.01931226
0.02194764	0.01999226
0.02330764	0.02053226
0.02448764	0.02094226
0.02548764	0.02121226
0.02630764	0.02134226
0.02678764	0.02138226
0.02712764	0.02131226
0.02727764	0.02101226

39 number of points on the suction side

-0.02119236	-0.02342774
-0.02105236	-0.02341774
-0.02075236	-0.02329774
-0.02026236	-0.02299774
-0.01962236	-0.02251774
-0.01884236	-0.02185774
-0.01796236	-0.02102774
-0.01696236	-0.02001774
-0.01586236	-0.01886774
-0.01464236	-0.01758774
-0.01330236	-0.01619774
-0.01185236	-0.01471774
-0.01030236	-0.01316774
-0.00867236	-0.01153774
-0.00695236	-0.00985774
-0.00517236	-0.00813774
-0.00333236	-0.00637774
-0.00145236	-0.00458774
0.00046764	-0.00278774
0.00239764	-0.00098774
0.00432764	0.00082226
0.00625764	0.00261226
0.00817764	0.00438226
0.01005764	0.00611226
0.01190764	0.00780226
0.01369764	0.00942226
0.01544764	0.01099226
0.01716764	0.01251226
0.01881764	0.01394226
0.02035764	0.01524226
0.02177764	0.01641226
0.02307764	0.01744226
0.02423764	0.01833226
0.02524764	0.01907226
0.02609764	0.01966226
0.02676764	0.02015226
0.02715764	0.02043226
0.02735764	0.02069226
0.02727764	0.02101226